nature cancer

Article

https://doi.org/10.1038/s43018-024-00841-x

Recapitulating the adenoma–carcinoma sequence by selection of four spontaneous oncogenic mutations in mismatch-repair-deficient human colon organoids

Received: 21 December 2022

Accepted: 23 September 2024

Published online: 01 November 2024

Check for updates

Tomohiro Mizutani[1,2,4,6], Matteo Boretto[1,2,6], Sangho Lim[1,2], Jarno Drost[2,3], Diego Montiel González[2,3], Rurika Oka[2,3], Maarten H. Geurts[1,2,3], Harry Begthel[1,2], Jeroen Korving[1,2], Johan H. van Es[1,2], Ruben van Boxtel[2,3] & Hans Clevers[1,2,3,5]

Carcinogenesis results from the sequential acquisition of oncogenic mutations that convert normal cells into invasive, metastasizing cancer cells. Colorectal cancer exemplifies this process through its well-described adenoma–carcinoma sequence, modeled previously using clustered regularly interspaced short palindromic repeats (CRISPR) to induce four consecutive mutations in wild-type human gut organoids. Here, we demonstrate that long-term culture of mismatch-repair-deficient organoids allows the selection of spontaneous oncogenic mutations through the sequential withdrawal of Wnt agonists, epidermal growth factor (EGF) agonists and the bone morphogenetic protein (BMP) antagonist Noggin, while *TP53* mutations were selected through the addition of Nutlin-3. Thus, organoids sequentially acquired mutations in *AXIN1* and *AXIN2* (Wnt pathway), *TP53*, *ACVR2A* and *BMPR2* (BMP pathway) and *NRAS* (EGF pathway), gaining complete independence from stem cell niche factors. Quadruple-pathway (Wnt, EGF receptor, p53 and BMP) mutant organoids formed solid tumors upon xenotransplantation. This demonstrates that carcinogenesis can be recapitulated in a DNA repair-mutant background through in vitro selection that targets four consecutive cancer pathways.

Colorectal cancer (CRC) remains one of the deadliest cancers[1]. CRC cases are divided into two major genetic instability categories; 85% of sporadic CRCs display chromosomal instability (CIN), while 15% of CRCs are hypermutated and display microsatellite instability (MSI)[2]. CIN tumors harbor combinations of common driver mutations in *APC*, *TP53*, *KRAS*, *SMAD4* and *PIK3CA* (ref. 3). Histologically, CRC develops through a well-described adenoma–carcinoma sequence, known as the 'Vogelgram' (ref. 4), which coincides with a relatively ordered acquisition of mutations in the previously mentioned genes. Hypermutated MSI CRC occurs in the context of the hereditary Lynch syndrome (LS), which is caused by germline mismatch repair (MMR) gene mutation, or as high-MSI (MSI-H) sporadic CRC caused by somatic MMR silencing typically associated with the $BRAF^{V600E}$ mutation[5,6]. Of note, the oncogenic driver mutations found in MSI-H CRC (*ACVR2A, TGFBR2, AXIN1, AXIN2, BMPR2* and *BRAF)* tend to be different from those in CIN CRC[3,7–12].

Recently, we and others introduced CRC driver genes into normal human colon organoids through clustered regularly interspaced short palindromic repeats (CRISPR)–Cas9 genome editing and demonstrated

A full list of affiliations appears at the end of the paper. e-mail: h.clevers@hubrecht.eu

that combined *APC*, *SMAD4*, *TP53*, *KRAS* and/or *PIK3CA* mutations transform colon epithelial organoids into full-blown cancer cells[13,14]. Indeed, subsequent in vivo experiments showed that the combination of these mutations enabled the modified organoids to metastasize to distant organs[15]. These data demonstrated that the sequential introduction of CRC driver mutations into human wild-type (WT) colon organoids does recapitulate the proposed Vogelgram of sequential histological changes toward CRC. While four different pathways (Wnt, epidermal growth factor (EGF), bone morphogenetic protein (BMP) and p53) were specifically targeted by CRISPR constructs, mutant organoids could be selected by removing the corresponding components from the medium (Wnt, R-spondin 1, EGF or the BMP inhibitor Noggin) or by adding the small-molecule p53 inhibitor Nutlin-3 (Nut3)[13,14]. These findings indicated that the carcinogenic CRC process exploits niche growth factor dependencies to transform normal cells into cancer cells. As said, the genes typically mutated in CIN cancers are less frequently altered in MMR-deficient hereditary CRCs and MSI-H hypermutated CRCs, while these MMR-deficient CRCs are known to harbor specific genetic mutations such as *ACVR2A*, *TGFBR2*, *RPL22*, *RNF43*, *AXIN1*, *AXIN2* and *BRAF* mutations[3,7–12,16].

Previously, we generated MMR-deficient human colon organoids with knockout (KO) of the *MLH1* gene and demonstrated that short-term in vitro culture could recapitulate the mutational signature of MMR-deficient CRCs[17]. *MLH1*, *MSH2*, *MSH6*, *PMS1* and *PMS2* have been identified as predisposing MMR pathway genes[18]. Of these, germline mutations in *MLH1* and *MSH2* are correlated with the highest risk of developing CRC in LS[19], while *MLH1* promotor hypermethylated silencing is the key mechanism for MMR-deficient hypermutated CRC[20,21]. We, therefore, chose to exploit the *MLH1*-mutant background for our study. Here, we build on this experimental approach by selecting spontaneous oncogenic mutations of *MLH1*-mutant organoids by removing the niche factor components Wnt, R-spondin 1, EGF and Noggin from the organoid culture medium or by adding the small-molecule p53 inhibitor Nut3. Thus, this study asks whether simple growth factor-based selection of MMR-deficient (yet otherwise WT) organoids would allow the derivation of full-blown colon cancer cells in vitro, potentially mimicking features of MSI-related CRCs.

Results

Wnt deprivation selects *AXIN1*-mutant and *AXIN2*-mutant organoids

On the basis of our previous study, we knew that *MLH1*^{KO} human colon organoids recapitulate the MMR-deficient phenotype in vitro and accumulate substantial numbers of substitutions and insertion or deletions (indels) during in vitro culture[17]. Withdrawal of Wnt3a and R-spondin 1 from the culture medium allowed us previously to select CRISPR-induced *APC* inactivation mutant organoids[13,22]. Here, we attempted to similarly select Wnt signal-independent *MLH1*^{KO} human colon organoids, yet without specific gene targeting (Fig. 1a). As expected, WT and *MLH1*^{KO} organoids rapidly died after single-cell seeding in a medium lacking Wnt3a and R-spondin 1 (−WR). This allowed us to recover rare *MLH1*^{KO} subclonal cells (*MLH1*^{KO}-1) from an *MLH1*^{KO} organoid line that was continuously cultured for ~350 days after single-cell cloning. No such subclones could be derived from two other *MLH1* mutation clones derived from the same donor (*MLH1*^{KO}-2 and *MLH1*^{KO}-3) (Fig. 1b,c). No Wnt-independent subclones could be isolated from the *MLH1*^{KO}-1 line at earlier time points (30, 100 and 200 days). Single surviving organoids were manually picked and expanded for downstream analysis (Fig. 1d). These organoid clones (*MLH1*^{KO}-1–WR-1 and *MLH1*^{KO}-1–WR-2) presented as dense and budding structures when cultured in −WR medium, whereas *APC*^{KO} organoids are reported to display a much more cystic structure[23,24]. Similar selections were performed using media designed to inhibit or activate key pathways of the stem cell niche (EGF receptor (EGFR), BMP and p53). Despite the limited initial clonal outgrowth, we could not establish long-term expanding cultures under these conditions, suggesting that no mutations affecting these pathways were present at this stage (Extended Data Fig. 1a,b). The emergence of surviving clones in the −WR condition was also observed in the *MLH1*^{KO} clonal line derived from another donor, which indicated this to be a reproducible phenomenon (Extended Data Fig. 1c,d).

The selected subclones (*MLH1*^{KO}-1–WR-1 and *MLH1*^{KO}-1–WR-2) were subjected to whole-genome sequencing (WGS) analyses. The genomic sequence of the parental *MLH1*^{KO}-1 clone allowed us to subtract somatic mutations that were already present in the parental clone (Fig. 1a). As expected from our previous study, surviving clones accumulated single-base substitutions (SBSs) (8,748 ± 149 mutations) and indels (23,010 ± 110 mutations), which recapitulated the mutator phenotype of MSI-H tumors with high tumor mutational burden (TMB) (Fig. 1e). The number of actual mutations and the previously calculated mutation number per genome division allowed us to calculate an estimated culture duration (354 ± 69 days)[17]. This matched our actual culture duration (417 days) well. The clonality of selected organoid clones was confirmed by variant allele frequency analyses (Extended Data Fig. 2). We compared the mutations acquired by the two surviving clones to the parental *MLH1*^{KO} clone. Among 6,372 base substitutions and 18,479 indels shared in two clones, we identified 74 base substitutions and 81 indels as nonsynonymous somatic coding mutations (Supplementary Table 1). Among those listed mutations, we found two compound heterozygous *AXIN1* mutations (c.1051C>T, p.Gln351* and c.1523 del, p.Gly508fs*197) and a homozygous *AXIN2* mutation (c.1994 del, p.Gly665fs*) carried in both subclones (Fig. 1e). These mutations are reported as hotspot mutations in the cBioPortal and in the Catalog of Somatic Mutations in Cancer (COSMIC) database as cancer-related somatic variants (COSM8405446, COSM1240884 and COSM1385326) (Extended Data Fig. 3). Biallelic loss-of-function mutations of both *AXIN1* and *AXIN2* lead to Wnt pathway activation and occur in CRC[25]. Indeed, a recent report confirmed that CRISPR KO of *AXIN1* of human intestinal organoids allows growth in the absence

Fig. 1 | Niche factor deprivation strategy successfully selected *AXIN1*-mutant and *AXIN2*-mutant organoids from *MLH1*^{KO} human colon organoids. **a**, Strategy to select the survived organoids with deprivation of Wnt pathway factors. Organoids were dissociated into single cells and then 200,000 single cells were cultured in niche-factor-deprived medium to select mutated stem cells (red) out from WT stem cells (blue) and differentiated cells (white). W, Wnt3a; R, R-spondin 1; N, Noggin; E, EGF. Surviving clone organoids were expanded briefly for WGS and WES analysis. Accumulated mutations were determined by subtracting the mutations in the original clone (blue) from the mutations in the selected subclone (red). **b**, WT organoids and *MLH1*^{KO}-1 organoids grew in complete medium (WRNE) but some of organoids grew out only from *MLH1*^{KO}-1 organoids in −WR medium (representative pictures from $n = 3$ clonal organoid lines). Scale bars, 500 µm. (**c**) Quantification of survived organoids in −WR medium. Mean and s.d. (error bars) of $n = 4$ clonal organoid lines. *P* values (two-sided Welch's *t*-test): *MLH1*^{KO}-1 versus *MLH1*^{KO}-2, $P = 0.0001$; *MLH1*^{KO}-1 versus *MLH1*^{KO}-3, $P = 0.0002$. **d**, Single survived organoids (*MLH1*^{KO}-1–WR-1 and *MLH1*^{KO}-1–WR-2) were expanded and passaged in −WR medium (representative pictures from $n = 3$ independent replicates). Scale bars, 500 µm. **e**, The Venn diagrams illustrate the number of base substitutions and indels found in WGS data of survived clones (*MLH1*^{KO}-1–WR-1 and *MLH1*^{KO}-1–WR-2). *AXIN1* and *AXIN2* candidate gene mutations are listed in the overlapping section. The numbers indicate nonsynonymous mutations and the numbers in brackets indicate all mutations found in WGS. **f**, RT–qPCR analysis of *AXIN2* mRNA levels. *AXIN2* transcripts were compared between each clone cultured in the medium with or without Wnt3a and R-spondin 1. Mean and s.d. (error bars) of $n = 3$ biologically independent experiments. *P* values (two-sided Welch's *t*-test): *MLH1*^{KO}-1 versus *MLH1*^{KO}-1–WR-1 in −WR medium, $P = 0.0048$; *MLH1*^{KO}-1 versus *MLH1*^{KO}-1–WR-2 in −WR medium, $P = 0.0037$. **g**, Representative images of Sanger DNA sequencing of *AXIN1* and *AXIN2* mutations in Wnt-independent clones (*MLH1*^{KO}-1–WR-1 and *MLH1*^{KO}-1–WR-2).

https://doi.org/10.1038/s43018-024-00841-x

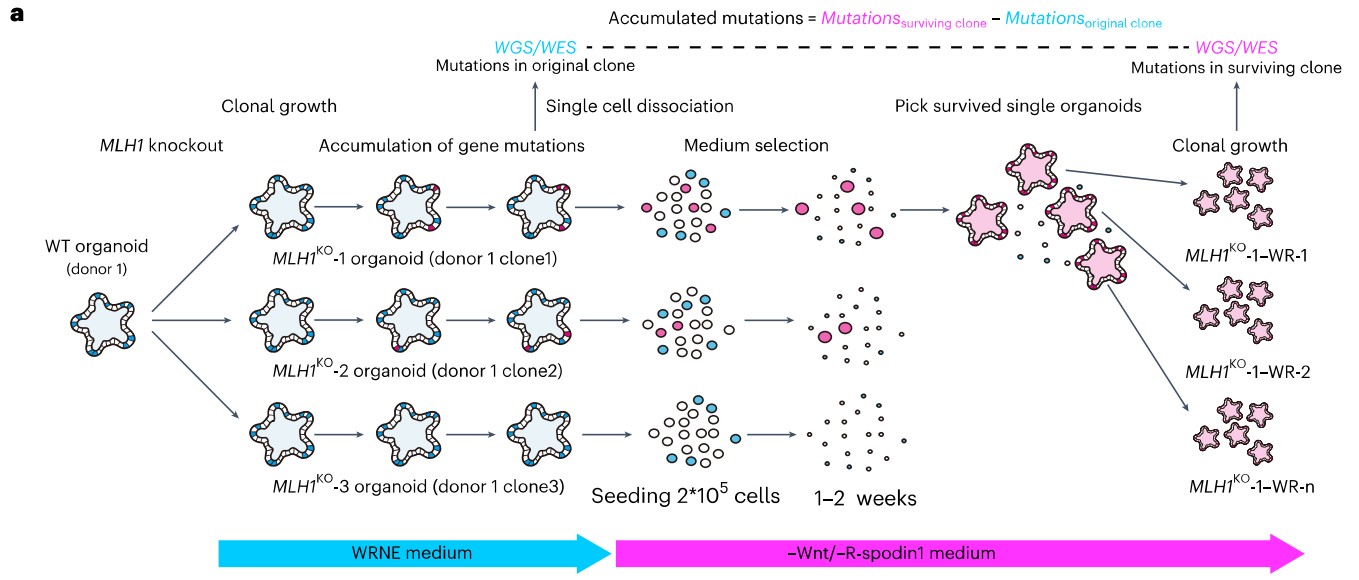

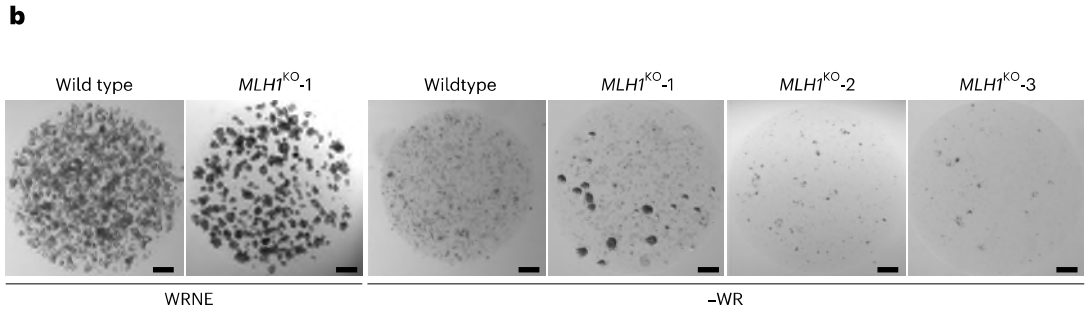

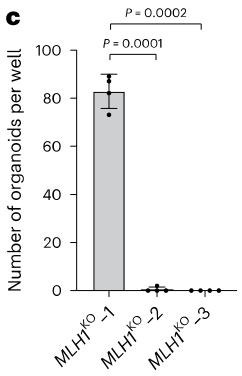

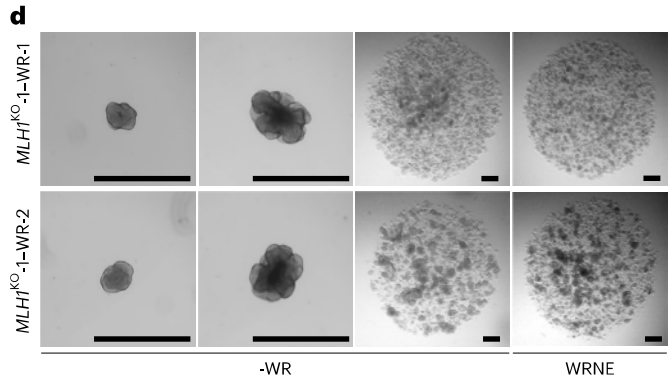

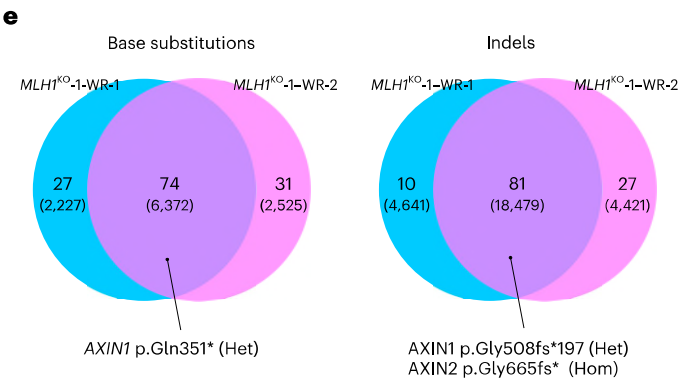

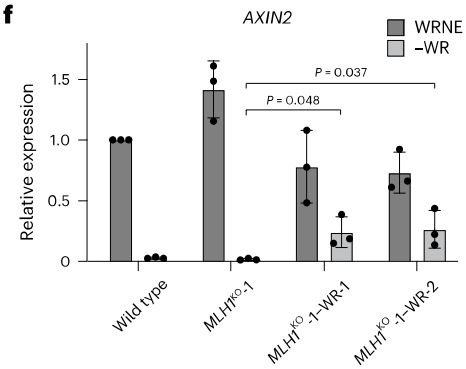

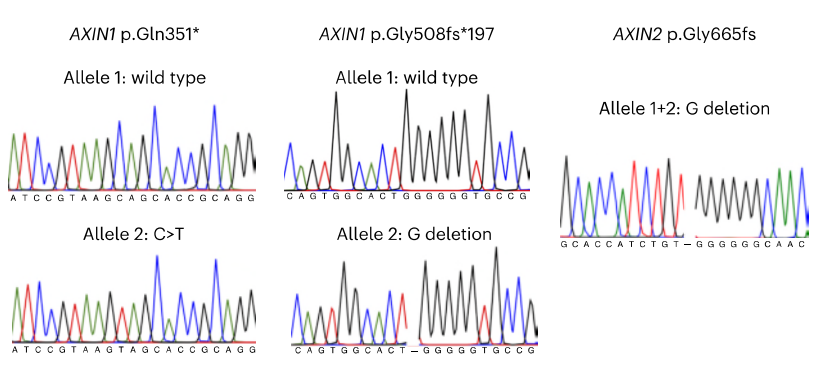

of Wnt and R-spondin 1, similar to *APC*^{KO} organoids[24]. In contrast, the common co-occurrence of *AXIN2* mutations with *AXIN1* and other Wnt pathway mutations suggests that weak pathway activation caused by *AXIN2* loss of function may synergistically upregulate Wnt signal[26–28].

We performed a medium selection experiment comparing the *AXIN*-mutant subclones with organoids that were CRISPR-engineered to carry mutations in other driver genes. This confirmed that organoids with *AXIN1* and *AXIN2* mutations upon *MLH1*^{KO} acquire the same Wnt signal independency as *APC*-mutant organoids (Extended Data Fig. 4). Wnt pathway activation was further confirmed by reverse transcription (RT)–qPCR analysis for the Wnt target gene *AXIN2*, as *AXIN2* was expressed at higher levels in the selected clones (*MLH1*^{KO}-1–WR-1 and *MLH1*^{KO}-1–WR-2) than in the WT and *MLH1*^{KO} clone without Wnt3a and R-spondin 1 (Fig. 1f). The SBS in *AXIN1* p.Gln351* (GCA>GTA) matched the MMR-linked mutational signature SBS 20 observed in *MLH1*^{KO} organoid[17,29]. Both *AXIN1* p.Gly508fs* and *AXIN2* p.Gly655fs* result from single-nucleotide deletion in homopolymer cytosine repeats, representative of the mutation pattern known as slippage in MMR-deficient and MSI-H tumors (Fig. 1g)[8,30]. Importantly, these types of *AXIN1* and *AXIN2* mutations are reported in MSI-H CRCs and gastric cancers[7–9,30,31]. Thus, *MLH1*^{KO} organoids allowed the faithful selection of some of the specific mutations seen in MMR-deficient and MSI-H tumors in in vitro culture.

Sequential mutant selections gain niche independence

Because these observations indicated that functional selection of spontaneous oncogenic mutations in *MLH1*^{KO} organoids allowed us to model MMR-deficient tumorigenesis in vitro, we performed sequential selection of these mutant clones (*MLH1*^{KO}-1–WR-1 and *MLH1*^{KO}-1–WR-2) in –Noggin, –EGF +gefitinib (–EGF+Gef) or +Nut3 medium. We, thus, hoped to find BMP pathway mutations, Ras and Raf pathway mutations and *TP53* mutations, respectively. Surviving organoids readily grew out from the *MLH1*^{KO}-1–WR-1 clone in the –Noggin condition. In contrast, only one organoid survived and grew into a large budding organoid from the *MLH1*^{KO}-1–WR-1 clone in +Nut3 medium (Fig. 2a,b). These surviving organoids were picked and clonally expanded for further genomic analyses (Extended Data Fig. 5). As expected, a missense mutation in *TP53* (c.473G>T, p.Arg158Leu (Hom)) was found in the Nut3-selected clone (*MLH1*^{KO}-1–WR-1+Nu) by whole-exome sequencing (WES), which was confirmed by Sanger sequencing. Aberrant p53 protein expression and increased p21 expression were confirmed by western blot (Fig. 2c). This *TP53* mutation is mostly reported in lung tumors but also seen in persons with CRC (Extended Data Fig. 3)[32,33].

Interestingly, the Noggin-independent clones arising from the *MLH1*^{KO}-1–WR-1 clone (*MLH1*^{KO}-1–WR-1–N) carried *ACVR2A* mutations (c.285 del, p.Thr96* (Hom)) or *BMPR2* mutations (c.255G>A, p.Trp85* (Het) and c.1748 del, p.Asn583fs* (Het)). *SMAD4* mutation, the most common BMP pathway driver mutation in sporadic CRC, was not encountered (Extended Data Fig. 3). Another Noggin-independent clone selected from the *MLH1*^{KO}-1–WR-2 clone (*MLH1*^{KO}-1–WR-2–N) also carried partially the same *ACVR2A* (c.285 del, p.Thr96* (Het) and c.1310 del, p.Lys437fs(Het)) and *BMPR2* (c.1748 del, p.Asn583fs* (Hom)) mutations. These mutations occurred through one nucleotide deletion in the polyadenine tract (*ACVR2* A_8, *BMPR2* A_{11}), as reported in MSI-H CRCs and recently defined as a representative indel mutational signature for MSI (ID2 signature)[3,10,12,29,34,35]. In particular, *ACVR2A* mutations were recently found and functionally validated as driver mutations for CRC[36]. The *BMPR2* mutation is reported to be mutually exclusive with *SMAD4* in sporadic CRC[34].

These double-mutant lines were selected again in additional conditions. Some surviving clones arose in –Noggin or –EGF+Gef medium from the *TP53* mutated clone (*MLH1*^{KO}-1–WR-1+Nu-1). Again, surviving organoids readily grew out in –Noggin medium (Fig. 2d,e). We selected two Noggin-independent clones in –Noggin medium and sent these for WES analyses (Extended Data Fig. 6). Interestingly, we confirmed that one (*MLH1*^{KO}-1–WR-1+Nu–N-1) acquired duplication of a somatic mutation in *ACVR2A* (c.285 del, p.Thr96*(Hom)) and the other one (*MLH1*^{KO}-1–WR-1+Nu–N-2) acquired compound heterozygous mutations in *ACVR2A* (c.285 del, p.Thr96*(Het) and c.1310 del, p.Lys437fs). As the earlier clone (*MLH1*^{KO}-1–WR-1+Nu-1) harbored a single *ACVR2A* (c.285 del, p.Thr96*) mutation, this means that the clone obtained another *ACVR2A* mutation during the selection step, resulting in loss of heterozygosity (LOH). Of note, this clone did not carry the *BMPR2* homozygous mutations observed in the previously selected Noggin-independent clones (*MLH1*^{KO}-1–WR-1–N, *MLH1*^{KO}-1–WR-2–N), suggesting that the clone acquired Noggin independency solely through LOH of the *ACVR2A* gene. This was consistent with the previous findings identifying *ACVR2A* as a driver gene in the transforming growth factor-β (TGFβ) pathway[36] and reporting the *BMPR2* as contributing cooperatively to the development of sporadic CRC but not as single driver mutation[10,34,37]. We again extracted mutational signatures from each selected clone. All clones showed the expected mutational spectra (Fig. 2f)[17]. We next extracted mutational signatures for comparison to the COSMIC database, using cosine similarity as a measure of closeness[29,38]. All selected organoids showed mutational signatures that resembled signatures SBS6, SBS15, SBS20 and SBS44, which are associated with defective DNA MMR (d-MMR) and occur in microsatellite unstable tumors[38] (Fig. 2g). Again, signature ID2 (representing the slippage of DNA MMR deficiency) was found in all mutant clones (Fig. 2h). These data clearly suggest that the mutational signature of d-MMR induced by *MLH1* mutation remained the dominant driver of mutagenesis regardless of the accumulated genetic mutations.

Long-term cultured d-MMR organoids complete tumor progression

As early attempts to select out mutant clones carrying EGF, Ras and Raf pathway mutations failed, we extended culturing times of the triple-pathway mutant clone (*MLH1*^{KO}-1–WR-1+Nu–N-1) up to 300 days to allow for the accumulation of further critical driver mutations. Recently, differential drug sensitivities of EGFR inhibition were reported among various different *RAS*-mutant patient-derived CRC organoids (PDOs). The pan-human EGFR inhibitor afatinib (Afa) can eliminate ERK activity oscillations in *KRAS*-mutant PDOs[39,40]. To select Ras and Raf pathway mutant clones more reliably, we used Afa as an alternative EGFR inhibitor in addition to Gef. Some organoids grew out in –EGF+Gef or –EGF+Afa conditions (Fig. 3a). These surviving organoids could be continuously expanded under both –EGF+Gef and –EGF+Afa conditions (Fig. 3b).

Through WES analyses, we found that surviving clonal organoids under both inhibitor conditions (*MLH1*^{KO}-1–WR-1+Nu–N–E+Afa/Gef) acquired a heterozygous somatic mutation in *NRAS* (c.181C>A, p.Gln61Lys(Het) COSM580) (Fig. 3c and Extended Data Fig. 6), a known oncogenic mutation in the Ras and Raf pathway[3,41]. While *KRAS* mutations are reportedly more common in low-MSI (MSI-L) relative to MSI-H CRC, the *NRAS* mutation is equally frequent between MSI-L and MSI-H CRC tumors[42]. To confirm that the selected *NRAS*^{Q61K} mutant organoids (*MLH1*^{KO}-1–WR-1+Nu–N–E+Afa/Gef) indeed exert constitutive ERK signaling activity, transcription of ERK target genes (*ETV4*, *ETV5*, *DUSP5*, *DUSP6* and *CCND1*) was compared between *NRAS*^{WT} and *NRAS*^{Q61K} mutant organoids by RT–qPCR (Extended Data Fig. 7a). Furthermore, western blot analysis confirmed that *NRAS*^{Q61K} mutant organoids increased phosphorylation of ERK1 and ERK2 (Fig. 3d). Taken together, we obtained quadruple-pathway mutant organoids, which sequentially acquired MSI-H mutations in *AXIN1* and *AXIN2* (Wnt pathway), *TP53*, *ACVR2A* and *BMPR2* (BMP pathway) and *NRAS* (Ras and Raf pathway) and, thus, became completely independent from the pertinent niche factors. Both triple-pathway and quadruple-pathway mutant organoids were highly proliferative and, as indicative of an active Wnt signaling pathway, accumulated expression of nuclear β-catenin (Fig. 3e). The quadruple-pathway mutant organoids appeared as more compact/

https://doi.org/10.1038/s43018-024-00841-x

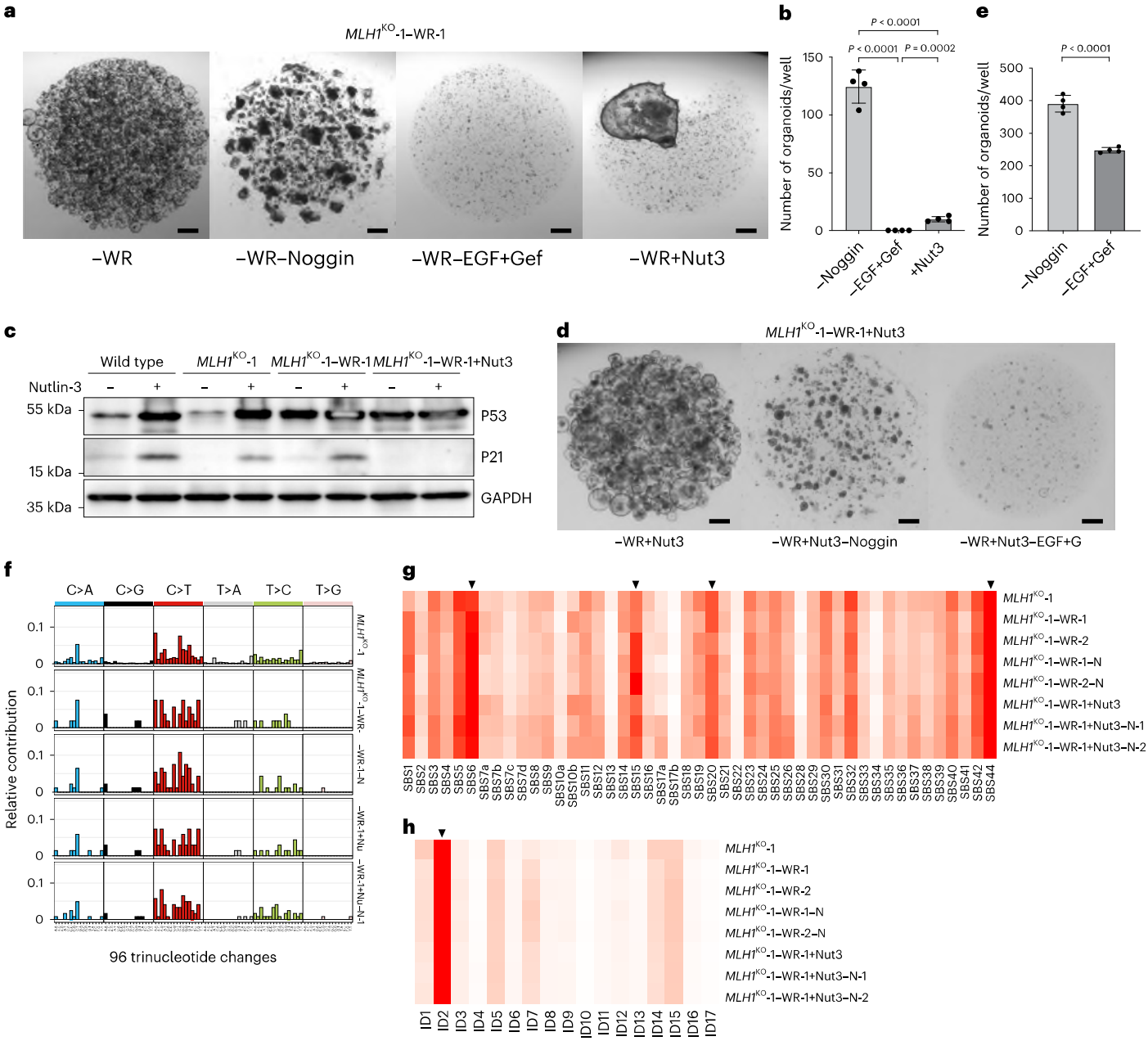

Fig. 2 | Further combinational mutant selection recapitulates sequential independence from niche factors. a, *MLH1*^{KO}-1–WR-1 organoid grew in –WR medium but some of organoids grew out in –WR–Noggin medium (representative pictures from $n = 3$ clonal organoid lines) and a single organoid grew out in –WR+Nut3 medium. Scale bars, 500 µm. All cells died out in –WR–EGF+Gef medium. **b**, Quantification of survived organoids in each selection medium. Mean and s.d. (error bars) of $n = 4$ clonal organoid lines. *P* values (two-sided Welch's *t*-test): –WR–Noggin versus –WR–EGF+Gef, $P < 0.0001$; –WR–Noggin versus –WR+Nut3, $P < 0.0001$; –WR–EGF+Gef versus –WR+Nut3, $P = 0.0002$. **c**, Representative western blot analysis to detect p53, p21 and GAPDH in WT and *MLH1*^{KO}-1 organoid lines with WT p53 (*MLH1*^{KO}-1 and *MLH1*^{KO}-1–WR-1) and with mutant p53 (*MLH1*^{KO}-1–WR-1+Nut3) treated with DMSO or 10 µM Nut3 for 24 h. The analysis was performed with $n = 2$ biologically independent experiments for one organoid clone. **d**, *MLH1*^{KO}-1–WR-1+Nut3 organoids were selected in –WR+Nut3–Noggin or –WR+Nut3–Noggin–EGF+Gef medium (representative pictures from $n = 3$ clonal organoid lines). Scale bars, 500 µm. **e**, Quantification of survived organoids in –Noggin and –EGF+Gef medium. Mean and s.d. (error bars) of $n = 4$ clonal organoid lines. *P* values (two-sided Welch's *t*-test). **f**, Mutational spectra of all base substitutions observed for each selected clone. **g**,**h**, Heat map showing the cosine similarity scores for each indicated clone and COSMIC SBS signature (**g**) and indel signature (**h**). Arrows indicate signatures associated with deficiency in DNA MMR in previous analyses[29,38].

less cystic structures as seen in our previous CRISPR-engineered quadruple-pathway mutant organoids[13]. To investigate the acquisition of drug resistance in the quadruple-pathway mutant organoids, we performed drug screening with various pathway inhibitors. We, thus, observed the expected sensitivity of *NRAS*^{WT} organoids toward Afa and Gef and the resistance of *NRAS*-mutant organoids. In contrast, the mutant organoids remained sensitive to the MEK inhibitors selumetinib and trametinib, the mTOR inhibitor everolimus, the PI3Kα inhibitor alpelisib and the multiple-CDK (cyclin-dependent kinase) inhibitor dinaciclib (Fig. 3f,g and Extended Data Fig. 7b–d). Recently, Ras status was reported to correlate with SH2 domain-containing phosphatase 2 (SHP2) inhibitor sensitivity in several cancers; in particular, the *NRAS*^{Q61K} mutation in neuroblastoma confers resistance to SHP2 inhibitors[43,44]. Consistent with this, our *NRAS*^{Q61K} mutant organoids

exhibited resistance to SHP2 inhibitor SHP099 treatment (Fig. 3f,g). We constructed a mutant phylogenic tree for each sequential mutant clone (Fig. 3h and Supplementary Table 3). The acquisition of identical mutations was independently observed in different clones. The available data indicated that these recurrent mutations arose independently yet were because of a shared mutational mechanism. Taken together, simple selection in an *MLH1*^{KO} mutant organoid background allowed the sequential isolation of spontaneous quadruple-pathway mutant organoids, starting from a single *MLH1*^{KO} stem cell, over a period of no more than 30 months.

MSI status and mutational tendency in d-MMR organoids

To assess the MSI profile of our MMR-deficient organoids, we compared the somatic mutations acquired in our quadruple-pathway mutant organoids to those of CRCs from The Cancer Genome Atlas (TCGA) database (TCGA-COAD). Leveraging two bioinformatic MSI predicting tools, MSMuTect and MANTIS[45–47], we derived MSI scores from WES data. Notably, MANTIS enabled the extraction of TCGA-COAD samples annotated as MSI-H and microsatellite-stable (MSS), facilitating group-specific comparisons. In the MANTIS analysis, the MSI scores of the quadruple-pathway mutant organoids mirrored those of the MSI-H group, significantly diverging from the MSS counterparts (Fig. 4a). This observation clearly indicated that *MLH1*^{KO} mutant organoids recapitulated the phenotype of MMR-deficient colorectal tumors. Furthermore, to evaluate the fidelity of the MSI-H tumor landscape in the MMR-deficient organoids, we checked whether the frequent microsatellite loci[48] of MSI-H cancers were targeted in our organoids. As expected, culturing of the mutant clones over time led to increased numbers of somatic mutations in the microsatellite loci found in MSI cancers (Fig. 4b). We then calculated the expected probability for acquiring specific mutations in in vitro cultured *MLH1*^{KO} organoids, taking into account the specific mutational signatures and the kinetics of mutation accumulation. First, by analyzing all mutational signatures in collected mutant clones, we visualized the 'average' mutational signature as the mutational frequency in 96 channels (Fig. 4c). The mutational signature of the mutant clones was compared to the mutational signatures of in vitro cultured organoids and in vivo tissue derived from small intestine and colon, as previously reported (Fig. 4d)[49]. Next, candidate mutations known as driver mutations in the Ras, Raf, MAPK, PI3K and ErbB pathways were listed from the previous report in MSI-H cancers[50]. The relative probability of occurrence in each specific mutation was calculated from the average mutational signature derived from the previous approach[51] and compared to the mutational rate in normal intestinal tissue and organoids (Fig. 5). As expected, *KRAS*^{G12D} and *KRAS*^{G12V}, known as the most frequent mutations in the Ras pathway, were unlikely to occur in an MMR-deficient background. *BRAF* mutations, which represent the most common mutations of the Ras and Raf pathway in sporadic MSI-H, were also calculated as being of low probability, which is consistent with a previous report that *BRAF*^{V600E} mutation frequency is low in MMR mutation carriers[3,5,52]. Selection in −EGF+Afa medium resulted in *NRAS*^{Q61K} mutation despite being previously reported as of lower probability albeit detected in MMR-deficient CRCs[53]. In contrast, the high relative probability of *AXIN1*^{Q351fs} corresponded to our selection result (described above). The *TP53*^{R158L} mutation found in our clone showed a relatively low probability, corresponding to the occurrence of a single surviving clone in the Nut3 selection step (Fig. 2a,b). The report of *TP53*^{R158L} mutations specifically in carcinogenesis related to inflammatory bowel disease suggests that the *TP53* mutation is influenced by various backgrounds and mutational signatures[32]. Despite the low probability of *TP53* mutations in our *MLH1*^{KO} mutant organoids, we were able to select a *TP53* missense mutation. Together, these data suggest that driver mutations inferred from the mutational signature are acquired with high probability while other oncogenic mutations with relatively low probability can also be acquired (albeit at lower frequency), shaping the genetic diversity of MSI-H CRCs.

Xenotransplantation of quadruple-pathway mutant organoids

To characterize the molecular features of the sequential mutant organoids, we compared the gene expression patterns for each mutated driver pathway. Given that the *NRAS*^{Q61K} mutant organoids (being the quadruple-pathway mutant clone) displayed niche factor independency for all four pathways, we compared gene expressions of each mutant clones cultured for 24 h in the condition that inhibited all four pathways (that is, in the absence of WRNE and in the presence of p53 activator Nut3, EGFR inhibitor Afa, Wnt antagonist Dickkopf 1 (DKK1) and BMP2 receptor ligand BMP2). Comparison of the representative gene expression patterns related to each pathway confirmed their activation by the specific gene mutations affecting each pathway in the sequential driver gene mutant clones (Fig. 6a). We then sought to investigate whether the spontaneous quadruple-pathway mutant clone was tumorigenic in vivo. To compare the tumorigenic activity between *NRAS*^{Q61K} and *KRAS*^{G12D}, the most prevalent mutation of sporadic CRCs and hypermutated CRCs in the Ras pathway, we introduced the *KRAS*^{G12D} activating mutation into our *NRAS*^{WT} triple-pathway mutant clone through previously used CRISPR–Cas9-mediated gene editing[13]. *KRAS*^{G12D} mutants were selected by withdrawing EGF and adding Gef to the culture medium (Extended Data Fig. 8a–c). Genotyping of clonally expanded organoids confirmed that the clone harbored the *KRAS*^{G12D} heterozygous mutation together with the acquired *AXIN1*, *AXIN2*, *TP53*, *ACVR2A* and *MLH1* mutations (Extended Data Fig. 8d). We subcutaneously injected triple-pathway mutants (*NRAS*^{WT}), quadruple-pathway mutants (*NRAS*^{Q61K}), triple-pathway + *KRAS*^{G12D} engineered mutants and the previously engineered AKPS (*APC*^{KO};*KRAS*^{G12D};*TP53*^{KO};*SMAD4*^{KO}) mutants derived from the same donor[13] into immunodeficient mice.

After 8 weeks, most of the mice injected with quadruple-pathway mutants, triple-pathway + *KRAS*^{G12D} engineered mutants and

Fig. 3 | MMR-deficient organoids acquired quadruple colorectal driver mutations in long-term culture. a, *MLH1*^{KO}-1–WR+Nu–N organoids were selected in –WRN+Nu–EGF+Afa/Gef medium (*MLH1*^{KO}-1–WR+Nu–N–E+Afa/Gef). Outgrowing clones are shown in the inset. Representative pictures from $n = 3$ independent replicates. Scale bars, 500 µm. **b**, Survived *MLH1*^{KO}-1–WRN+Nu–EGF+Afa/Gef organoids were picked up and continuously expanded in each selection medium. Representative pictures from $n = 3$ clonal organoid lines. Scale bars, 500 µm. **c**, Sanger DNA sequencing result of *NRAS*^{Q61K} (Het) mutation in the selected clone (*MLH1*^{KO}-1–WR+Nu–N–E+Afa). **d**, Representative western blot analysis to detect p44/42 MAPK and β-actin in *NRAS*^{WT} and *NRAS*^{Q61K} organoid lines cultured in WRNE medium or –WRNE medium + 10 µM Nut3 and 1 µM Afa. The analysis was performed with $n = 2$ biologically independent experiments for one organoid clone. **e**, Representative H&E staining and IHC analysis of E-cadherin, Ki67, β-catenin and EGFR in the parental clone (*NRAS*^{WT}) and the mutant clone (*NRAS*^{Q61K}). The analysis was performed with $n = 2$ clonal organoid lines. Scale bar, 100 µm. **f**, Dose–response curves showing the sensitivity of *NRAS*^{WT} and *NRAS*^{Q61K} clones to inhibitors of the EGFR (Afa), MEK (selumetinib) and SHP2 (SHP099). The *y* axis represents the viability of the samples while the *x* axis represents the drug concentration (power of 10 µM). Mean and s.d. (error bars) of $n = 3$ technical replicates for $n = 2$ independent organoid clones for each genetic background. **g**, Heat maps reporting the viability of the drug screening performed on *NRAS*^{WT} and *NRAS*^{Q61K} organoids as normalized to vehicle-treated organoids. Color mapping ranges from low viability (red) to high viability (green). The analysis was performed with $n = 3$ technical replicates for $n = 2$ independent organoid clones for each genetic background. **h**, Timescale phylogenic tree of the selected mutant clones that arose from the *MLH1*^{KO}-1 single organoid clone. Organoids were selected under each condition (colored rectangles). Circles represent survived clones and dashed-line circles represent nonrecovered clones. Horizontal bars indicate the culture duration of cloning and expanding each clone. All mutations in each clone are listed in Supplementary Table 3.

https://doi.org/10.1038/s43018-024-00841-x

AKPS-mutant organoids developed visible nodules. By contrast, some of the mice injected with triple-pathway mutants showed very small nodules. Compared to tumors of triple-pathway mutants, quadruple-pathway mutant tumors were larger and well vascularized (Fig. 6b,c). Tumor size analysis confirmed that some of the triple-pathway organoids engrafted but remained small, while the quadruple-pathway mutant clones had a higher rate of tumor formation and larger tumor size. No significant differences were found between *KRAS*^{G12D} engineered mutant clones and the *NRAS*^{Q61K} mutant clones (Fig. 6d). Histological analysis revealed that triple-pathway tumors grew as thin, cystic organoids encapsulated in the injected subcutaneous region, while quadruple-pathway tumors were larger

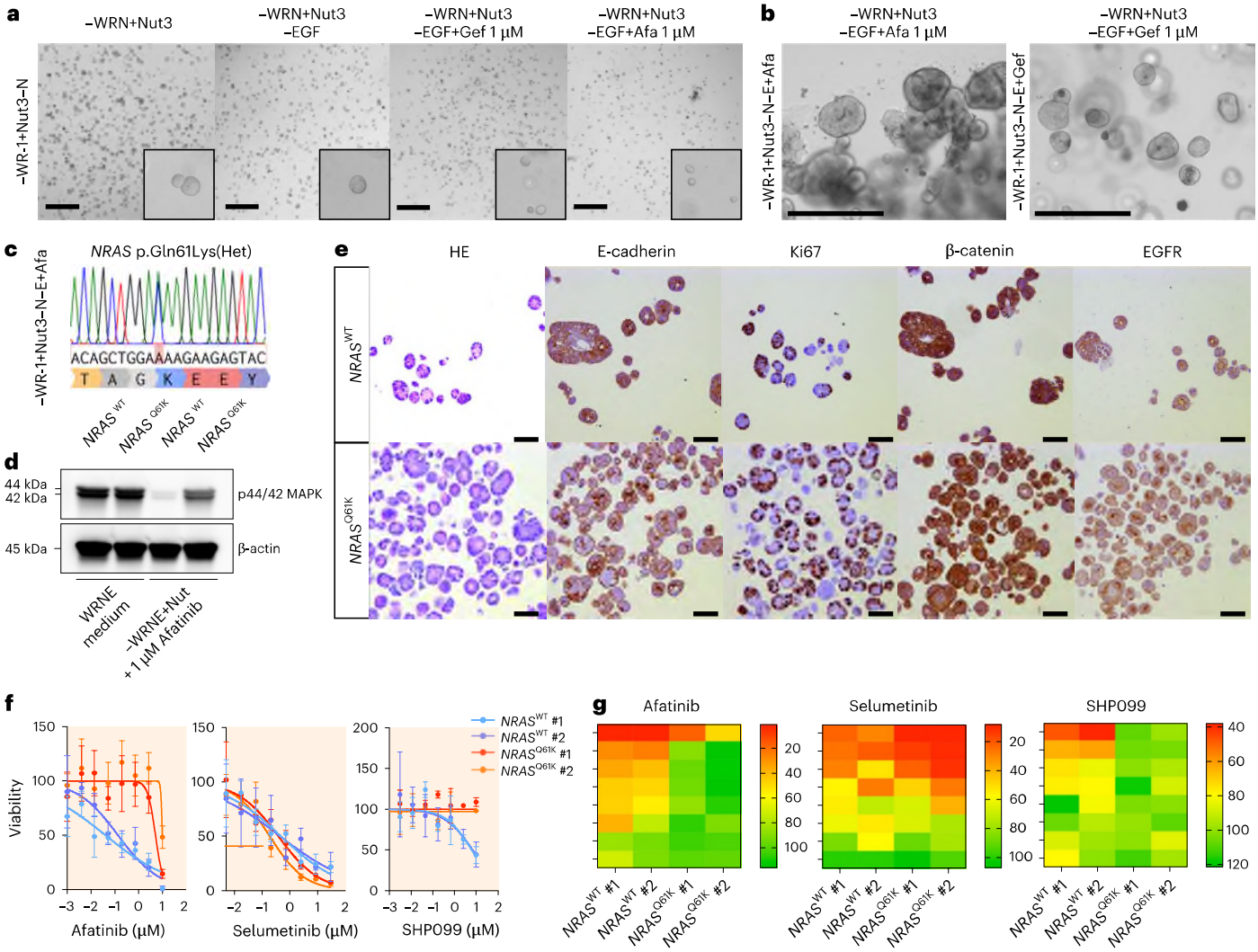

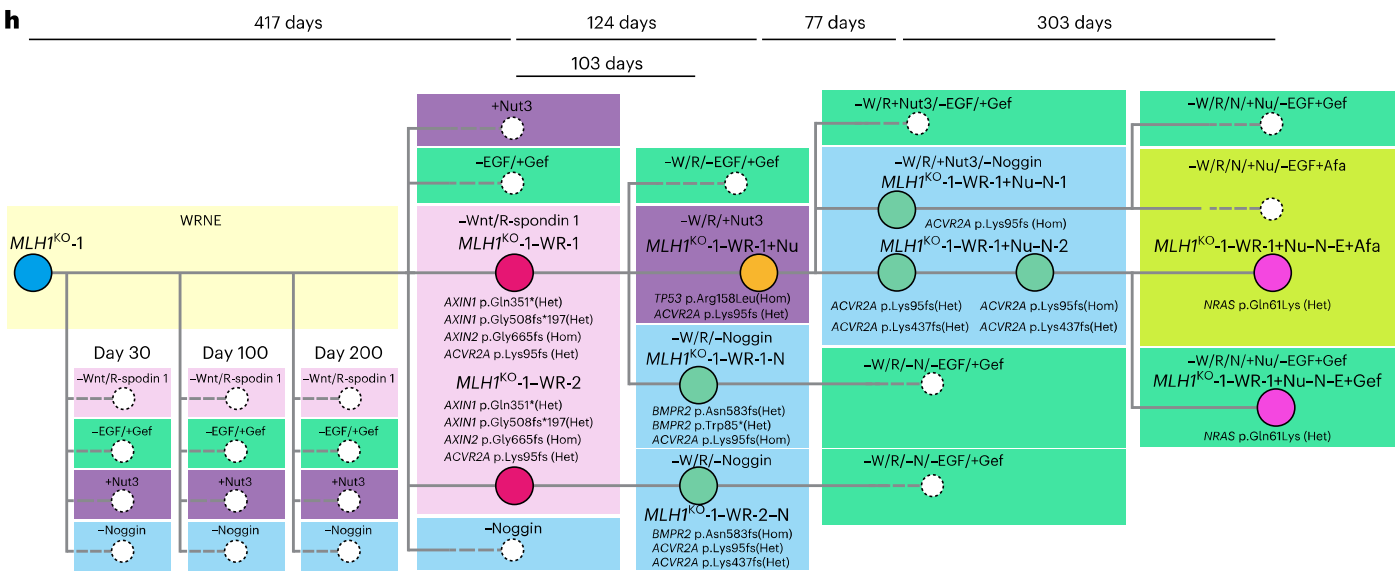

https://doi.org/10.1038/s43018-024-00841-x

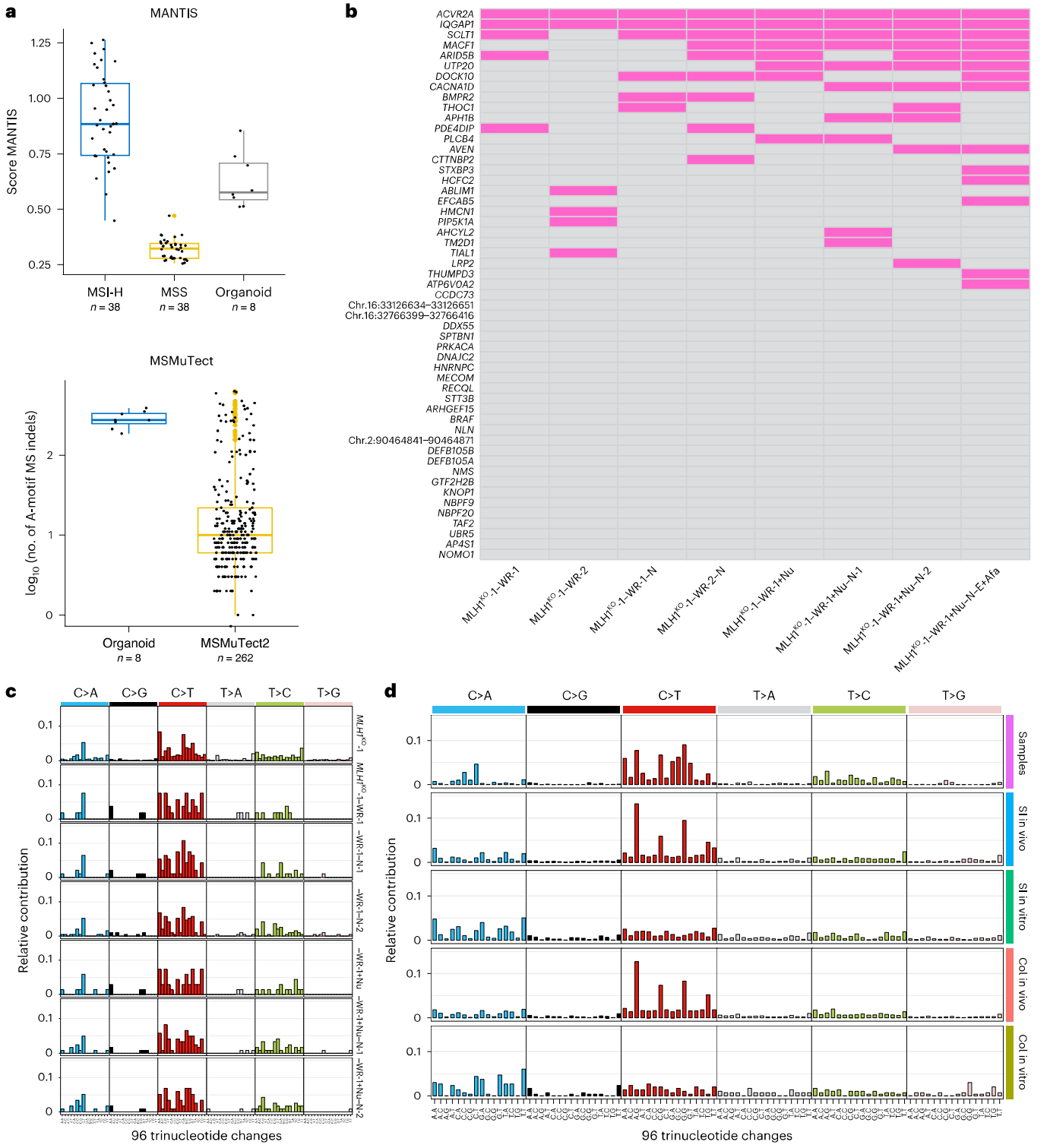

Fig. 4 | Signatures of MSI in mutant organoids. a, MANTIS scores were calculated in the mutant organoid clones ($n = 8$ samples) and MSI-H ($n = 38$ samples) and MSS ($n = 38$ samples) of TCGA-COAD. We used the stepwise difference threshold set by MANTIS, which defines a score above 0.4 as MSI-H (unstable) and below this threshold as MSS (low) using TCGA-COAD. MSMuteTect2 scores were also calculated in the mutant organoid clones ($n = 8$ samples) and all samples used in TCGA as MSMuTect2 ($n = 262$ samples). The minimum values are the smallest number per MANTIS and MSMuTect2 scores. Sample numbers are written below each group. The first quartile above the whiskers represents the data point that separates the lowest 25% of the data from the rest. The center line per box plot represents the median value among the data points. The third quartile just on top of the box plot separates the lowest 75% of the data points from the highest 25%. The maximum value represents the largest score of each tool. **b**, MSI mutations (pink, mutated) harbored in each mutant organoid clone (columns). The top 50 most differentially unstable microsatellite loci (rows) were selected from the previous study[48]. **c**, Mutational spectra of all base substitutions observed for each selected clone. **d**, The average mutational signature of the mutant clones extracted from **c** are shown on top (samples). The mutational signatures of in vitro cultured organoids and in vivo tissue derived from the small intestine (SI) and colon (Col) were referred from the previous result[49].

https://doi.org/10.1038/s43018-024-00841-x

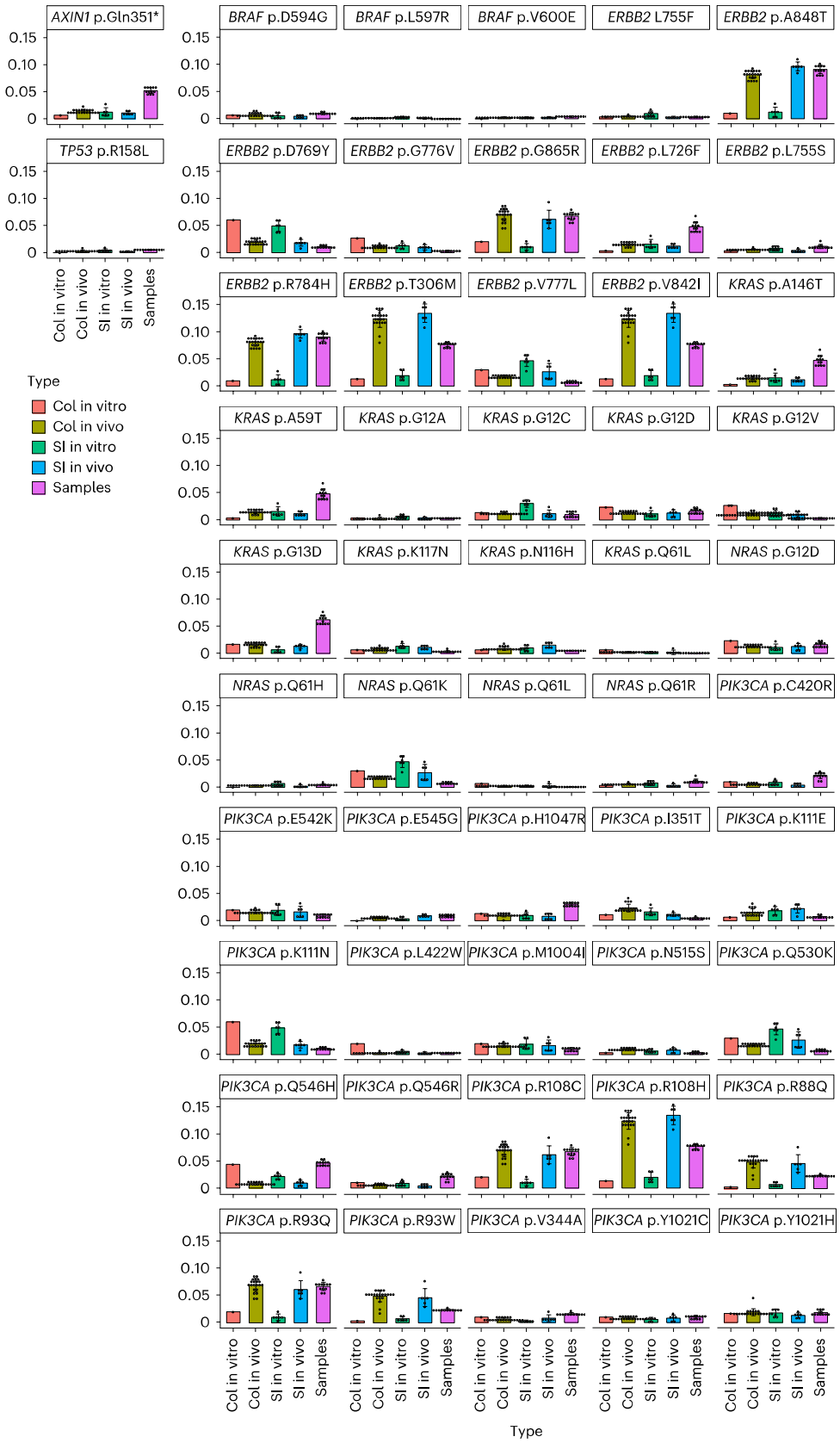

Fig. 5 | Relative risks for specific driver mutations in mutant organoids. Relative risk of frequent driver mutations for Ras, Raf, MAPK, PI3K and ErbB pathways listed from the previous report in MSI-H cancers[50]. Each mean relative risk was calculated from mutational signatures of normal human colonic organoid (C in vitro, $n = 1$), normal human colonic tissue (C in vivo, $n = 21$), normal human small intestinal organoid (SI in vitro, $n = 6$), normal human small intestinal tissue (SI in vivo, $n = 14$) and the average mutant organoids (samples, $n = 12$). Left, SBS mutations found in the mutant organoids (*AXIN1*^{Q351*} and *TP53*^{R158L}) are shown together. Data are presented as mean values ± s.d.

https://doi.org/10.1038/s43018-024-00841-x

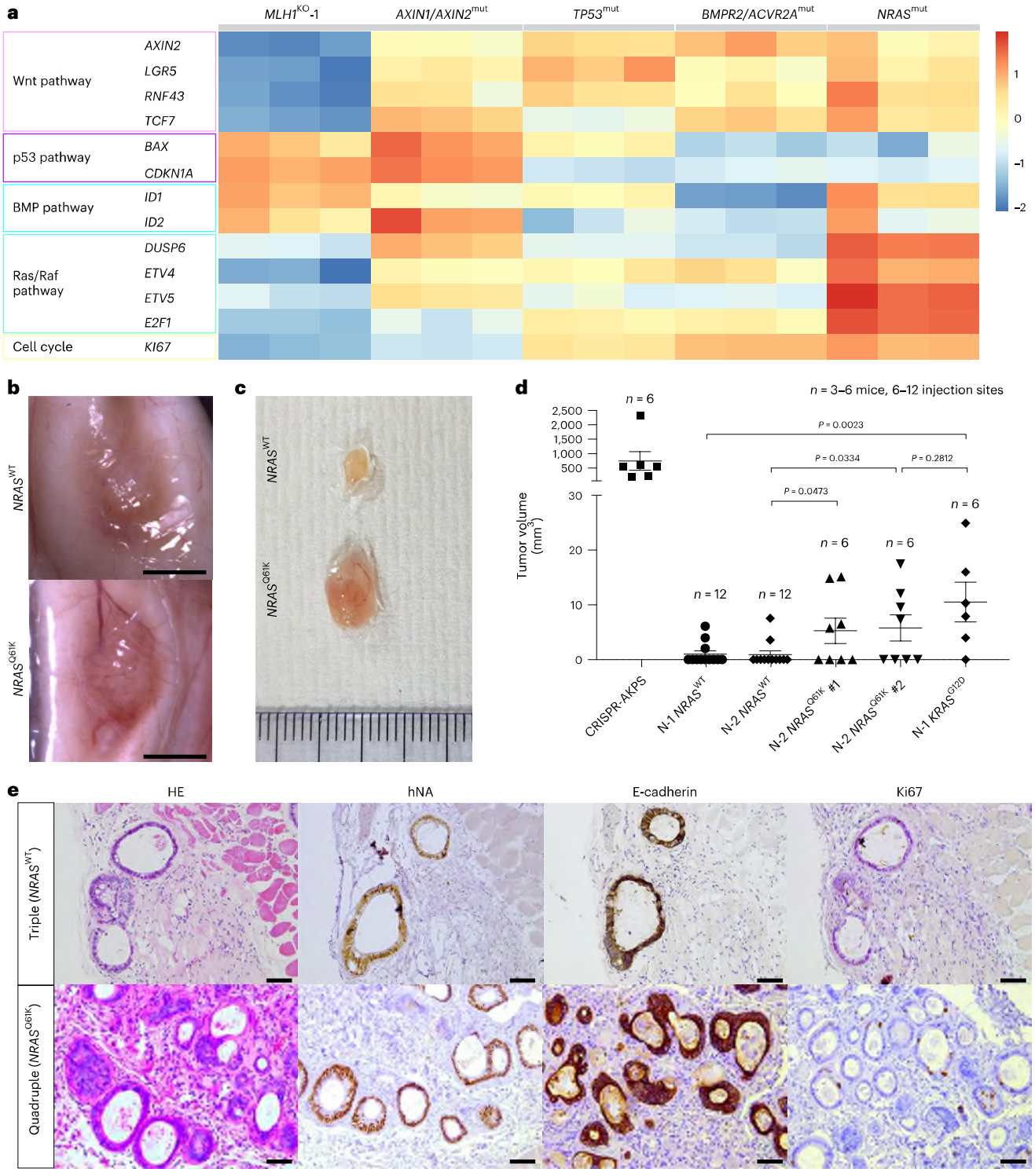

Fig. 6 | Quadruple-pathway mutant organoids grow as colorectal carcinomas in vivo. a, Heat map diagram of expression levels for each representative genes in CRC driver pathways. Columns and rows in the heat map represent mutant clones and genes, respectively. Color scale indicates fold changes in gene expression ($n = 3$ clonal organoid lines). **b**, Triple-pathway mutant organoids ($NRAS^{WT}$) and quadruple-pathway mutant organoids ($NRAS^{Q61K}$) were injected subcutaneously in NSG immunodeficient mice. Both triple-pathway mutant ($NRAS^{WT}$) and quadruple-pathway mutant ($NRAS^{Q61K}$) organoids developed visible nodules. $NRAS^{Q61K}$ organoids grew as tumors with vasculature in the subcutaneous lesion. Representative pictures from $n = 6$–12 tumors. Scale bars, 5 mm. **c**, Representative images of extracted tumors of $NRAS^{WT}$ organoids (top) and $NRAS^{Q61K}$ organoids (bottom). Representative pictures from $n = 6$–12 tumors. **d**, Tumor size measurement of xenografts at 8 weeks after xenotransplantation. Mean and s.e.m. (error bars) of $n = 6$–12 tumors. P values (two-sided Welch t-test): N-1 $NRAS^{WT}$ versus N-1 $KRAS^{G12D}$, $P = 0.0023$; N-2 $NRAS^{WT}$ versus N-2 $NRAS^{Q61K}$ 1, $P = 0.0473$; N-2 $NRAS^{WT}$ versus N-2 $NRAS^{Q61K}$ 2, $P = 0.0334$; N-2 $NRAS^{Q61K}$ 2 versus N-1 $KRAS^{G12D}$, $P = 0.2812$. **e**, Representative H&E stain, hNA, E-cadherin and Ki67 immunostaining on nodules isolated from triple-pathway mutant ($NRAS^{WT}$) and quadruple-pathway mutant ($NRAS^{Q61K}$) injected mice. Triple-pathway mutant organoids did engraft but remained thin with a cystic structure of organoids, similar to adenoma features. Quadruple-pathway mutant organoid-derived tumors showed a thick and irregular multilayered epithelium. The analysis was performed on $n = 3$ tumors. Scale bars, 100 mm.

and all exhibited an irregular multilayered epithelium. The tumor origin was confirmed using a human-specific nuclear antigen (hNA) (Fig. 6e). These data implied that *MLH1*^{KO} organoids carrying quadruple-pathway mutations (Wnt, EGFR, p53 and BMP) form malignant tumors upon xenotransplantation. Notably, a comparison of growth rates during in vitro culture confirmed no apparent difference between AKPS-mutant organoids and the quadruple-pathway mutant organoids (Extended Data Fig. 9a,b). The AKPS organoid line was engineered to carry the strongest mutations in each of the four pathways, while the quadruple-pathway mutant *MLH1*^{KO} carries much weaker versions. We do not know how each of these mutations contributes to the observed in vivo growth difference, yet they apparently add up to a notably more malignant phenotype of the AKPS organoids upon transplantation.

Discussion

Here, we apply long-term culture of *MLH1*^{KO} organoids with sequential clonal selection for CRC driver mutations using niche factor deprivation in an attempt to obtain spontaneous tumor organoids in vitro. Previously, we demonstrated that CRISPR-mediated KO of the *MLH1* gene in human colon organoids recapitulates the mutational signature of MMR-deficient tumors even in short-term culture[17]. We now extend this experimental approach by using MMR-deficient organoids in long-term culture to recapitulate the acquisition of CRC driver mutations by clonal selection using niche factor selection. Organoid culture is now a well-established method for the robust culture of normal human epithelial stem cells in vitro, which typically remain genetically stable during prolonged culturing[54]. On the other hand, tumor organoids retain the genetic mutations and phenotypic characteristics of the original tumor[55,56]. Having said this, SBSs and indels stochastically occur in human intestinal organoids, just as these occur in human adult stem cells over time[17,49].

MLH1^{KO} intestinal organoids acquire mutations at an accelerated rate compared to normal stem cells and the resulting mutation spectrum mimics the characteristic mutational signature seen in MSI-H CRCs[17]. As mutations accumulate at a considerably faster rate than in normal tissues, this suggests that *MLH1*^{KO} organoids can be used as an in vitro model for MSI-H tumorigenesis. After nearly 1 year of in vitro culture, we were able to isolate clones with oncogenic mutations in *AXIN1* and *2*, negative regulators of the Wnt pathway. Such mutations are generally considered to establish the first step in colon tumorigenesis. Further selection identified oncogenic mutations in *ACVR2A* and *BMPR2* upon BMP inhibition, *TP53* upon Nut3 selection and *NRAS* upon EGF and Ras pathway inhibition. All observed mutations fit the MMR-deficient mutational signature and the single-base slippage patterns, as these occur in MSI-H tumors. These results, thus, imply that *MLH1*^{KO} organoids faithfully recapitulate the specific mutational patterns of MMR-deficient and MSI-H tumors. Organoid culture is based on the in vitro recapitulation of stem cell niche factor conditions and it has been shown previously that tumor organoid culture condition reflects independency from the niche factors[13,14,55,57]. Consistent with these reports, quadruple-pathway mutant clones isolated in this study were tumorigenic in vivo upon subcutaneous transplantation.

Our approach has some limitations. As only pure epithelial cell components can be evaluated in tumor epithelial organoids, the organoid culture system used in this study is limited in its ability to replicate the tumor microenvironment or high neoantigen immune response observed in MSI-H tumors. T cell infiltration in the rectal mucosa of persons with LS was recently reported to shape carcinogenesis regardless of mutation burden[58]. Indeed, the abnormal immune environment in LS was proposed to represent the initial step of MMR-deficient cancer[59]. Because of the time and scale constraints in our experimental scheme, we were not able to assess different combinations of driver mutations or various patterns of mutational acquisition order. However, the conservation of the d-MMR mutation signature in all progeny clones of *MLH1*-mutant organoids suggests that the d-MMR mutation signature derived from *MLH1* mutation is strongly retained as the mutation signature shaping the tendency to acquire subsequent mutations, regardless of accumulated genetic mutations, suggesting that the mutation signature, rather than the acquired gene mutation, is the strongest factor influencing the propensity to acquire mutations. Indeed, a recent report showed that long-term culturing of TP53-deficient gastric organoids leads to a CIN phenotype[60], but not to the sequence changes observed in the current study. Our approach is not easily generalizable to other tumor types. CRC appears relatively unique in that the four most commonly mutated pathways can be easily and specifically selected for: Three of these pertain to growth factor dependencies (Wnt, EGF and BMP), while Nut3 allows for selection of mutations in the fourth pathway (TP53).

To our knowledge, this study provides the example of the derivation of full-blown cancers from WT cells, simply by providing selective pressure for four well-defined oncogenic pathways. We chose to perform our study in an *MLH1*-mutant background, which has an increased rate of accumulation of genetic mutations and is well known to confer CRC predisposition. Similar approaches with WT cells or with organoids carrying other cancer predisposing mutations will likely yield similar results.

Methods

Ethics statement

The study was approved by the UMC Utrecht and Diakonessenhuis ethical committee (TC-Bio 12-093) and was in accordance with the Declaration of Helsinki and according to Dutch law. This study is compliant with all relevant ethical regulations regarding research involving human participants.

Animals

All mouse experiments were conducted under a project license (AVD 8010020209924) granted by the Central Committee Animal Experimentation of the Dutch government and approved by the KNAW–Hubrecht Institute Animal Welfare Body (HI 21.39.04). NOD *scid* gamma (NSG; NOD.Cg-*Prkdc*^{scid} *Il2rg*^{tm1Wjl}/SzJ; 8 weeks old) mice were used in the study. The mice were kept in a constant-temperature environment of 21 °C (40–60% humidity) with a natural day–night light cycle in a conventional animal colony with free access to food and water. All mice were housed in a pathogen-free vivarium in sterile, disposable microisolator cages and fed a sterile, irradiated diet with free access to sterile, irradiated water.

All the mice were monitored and weighed once a week. Mice with symptoms of severe discomfort (for example, >20% weight loss compared to beginning or >15% weight loss in 2 days) with tumor burden or with measured tumors larger than 1,000 mm^3 were humanely killed. In this study, three mice in the subcutaneous transplantation experiment were killed with the estimation of exceeded maximal tumor burden at an earlier time point. As tumor size was weekly checked by manual palpation, it was only possible to estimate the size of the tumors ahead of killing. Indeed, we noted that $n = 1$ tumor of the killed animals exceeded the size limit.

Organoid culture establishment

MLH1^{KO} colon organoids were established from two WT human colon organoid cultures in a previous study[17]. These were derived from endoscopy material of a healthy donor (female, age 31 years)[15] and from the normal tissue of a resected colon segment derived from a person (female, age 60 years) diagnosed with CRC (sigmoid)[55]. As the differences by sex in mutational progression were not expected, we did not consider sex or gender in our study design. Organoid culture establishment and medium conditions were described previously[13]. Briefly, basal culture medium (AdDMF+++) contained advanced DMEM/F12 (Invitrogen) supplemented with 10 mM HEPES, 2 mM GlutaMAX, 100 U per ml penicillin and 100 µg ml^{-1} streptomycin. The culture

medium (WRNE) contained AdDMF+++ including B27 (Invitrogen), nicotinamide (Sigma-Aldrich), *N*-acetylcysteine (Sigma-Aldrich), Noggin (Peprotech), R-Spondin 1-conditioned medium (20%, produced using R-spondin 1 cells (Trevigen)), EGF (Peprotech), Wnt3a-conditioned medium (50%, produced using stably transfected L cells), TGFβ type I receptor inhibitor A83-01 (Tocris) and p38 inhibitor SB202190 (Sigma-Aldrich). Organoids were embedded in domes of Cultrex β-mercaptoethanol (BME; Trevigen) and covered by culture medium (WRNE). Established *MLH1*^{KO} colon organoids were cultured in two wells of a six-well plate (480 µl of BME, approximately 160,000–200,000 cells before passaging). Organoids were passaged weekly at a 1:2 split ratio, keeping multiclonal cell diversity without selective pressure.

Organoid selection

Organoids were dissociated into single cells using TrypLE Express (Thermo Fisher Scientific) in the presence of 10 µM Y-27632 (Tocris Bioscience) for 20 min and mechanically dissociated into single cells. A total of 120,000 single cells were counted, centrifuged at 600*g* for 1 min, resuspended in 240 µl of Cultrex BME and seeded at low density on a prewarmed six-well culture plate (Corning). Survived organoids derived from single cells were manually picked up, resuspended in 20 µl of Cultrex BME and seeded on a 48-well culture plate (Corning). Clonally selected organoids were cultured in selection medium to confirm as they grow in that culture condition. For selection of Wnt pathway or BMP pathway mutants, organoids were grown in culture medium lacking Wnt3a-conditioned medium and R-spondin 1-conditioned medium or Noggin, respectively. For mutant p53 selection, organoids were cultured in the presence of 10 mM Nut3 (Cayman Chemical) and maintained in the presence of 1 mM Nut3. For selection of Ras and Raf pathway mutants, organoids were grown in culture medium lacking EGF and containing 1 µM Gef (Selleck Chemicals) or 1 µM Afa (Selleck Chemicals).

WGS and WES

Individual outgrowing organoids surviving the medium-based selection were manually picked and propagated as clonal lines for a couple of passages to avoid unexpected mutation accumulation before being harvested for WGS and WES. In brief, organoids were collected in ice-cold AdDMF+++, centrifuged at 400*g* for 3 min and washed twice in ice-cold PBS to ensure the removal of all remaining BME. The DNA was extracted using the Quick-DNA miniprep kit (Zymo research, D3024) following the manufacturer's instructions. Then, 1 µg of DNA was used for WES performed with the Agilent SureSelect V7 kit, using 8 Gb per sample (50× average mapped) data throughput, with 150-bp paired-end sequencing on NovaSeq. Sequence reads were mapped against human reference genome GRCh37 using the Burrows–Wheeler Aligner version 0.7.17 mapping tool[61] with settings 'bwa mem -c 100 -M'. Sequence reads were marked for duplicates using Sambamba version 0.6.8 and realigned per donor using the Genome Analysis Toolkit (GATK) version 4.13.0. A description of the complete data analysis pipeline is available on GitHub (https://github.com/ToolsVanBox/NF-IAP). Raw variants were called in multisample mode using the GATK HaplotypeCaller and GATK-Queue with default settings and additional option 'EMIT_ALL_CONFIDENT_SITES'. The quality of variant and reference positions was evaluated using GATK VariantFiltration with options '--filter-expression QD < 2.0 --filter-expression MQ < 40.0 --filter-expression FS > 60.0 --filter-expression HaplotypeScore > 13.0 --filter-expression MQRankSum < 12.5 --filter-expression ReadPosRankSum < 8.0 --filter-expression MQ0 R 4 && ((MQ0/(1.0 * DP)) > 0.1) --filter-expression DP < 5 --filter-expression QUAL 4.0 --filter-name SNP_LowQualityDepth --filter-name SNP_MappingQuality --filter-name SNP_StrandBias --filter-name SNP_HaplotypeScoreHigh --filter-name SNP_MQRankSumLow --filter-name SNP_ReadPosRankSumLow --filter-name SNP_HardToValidate --filter-name SNP_ LowCoverage --filter-name SNP_VeryLowQual --filter-name SNP_LowQual --filter-name SNP_SOR -cluster 3 -window 10'. To obtain high-quality somatic mutation catalogs, the somatic variant filtering tool SMuRF (https://github.com/ToolsVanBox/SMuRF) was applied. We applied postprocessing filters as described[49,62,63]. Somatic variants that passed all these filters were annotated with 'PASS' or with the respective parameter that did not meet any of the previous thresholds. All samples are listed in Supplementary Table 2.

Mutation calling and filtering

Raw variants were called in multisample mode using the GATK HaplotypeCaller version 3.4-46 (ref. 64) and GATK-Queue version 3.4-46 with default settings and additional option 'EMIT_ALL_CONFIDENT_SITES'. The quality of variant and reference positions was evaluated using GATK VariantFiltration version 3.4-46 with options '--snpFilterName LowQualityDepth --snpFilterExpression QD < 2.0 --snpFilterName MappingQuality --snpFilterExpression MQ < 40.0 --snpFilterName StrandBias --snpFilterExpression FS > 60.0 --snpFilterName HaplotypeScoreHigh --snpFilterExpression HaplotypeScore > 13.0 --snpFilterName MQRankSumLow --snpFilterExpression MQRankSum < −12.5 --snpFilterName ReadPosRankSumLow --snpFilterExpression ReadPosRankSum < −8.0 -cluster 3 -window 35'. To obtain high-quality somatic mutation catalogs, we applied postprocessing filters as described[49]. Briefly, we considered variants at autosomal chromosomes without any evidence from a paired control sample (mesenchymal stem cells isolated from the same bone marrow), passed by VariantFiltration with a GATK phred-scaled quality score that was ≥100 for base substitutions and ≥250 for indels, a base coverage of at least 20× in the clonal and paired control sample, no overlap with single-nucleotide polymorphisms (SNPs) in the SNP Database version 137.b3730 and absence of the variant in a panel of unmatched normal human genomes. We additionally filtered to exclude in vitro accumulated mutations as described[49,62,63]. All mutations are listed in Supplementary Table 3.

Driver mutations

SBSs or indels were considered as driver mutations if they had an MQ of 30, had a minimum of 10× base coverage or were found in the driver genes COSMIC cancer gene consensus (version from 9 May 2019). Additionally, these driver mutations were annotated as missense, frameshift, stop-gain, insertion or deletion, had either a high or moderate effect as annotated by SnpEff and were not in the SNP Database version 146 or a panel of unmatched normal human mesenchymal stem cells and fetal genomes (BED file available upon request).

Mutational signature analysis

Mutational patterns was used for the SNV signature analysis with the developed R package (MutationalPatterns)[65], First, we extract the 96-trinucleotide mutational count matrix from the somatic mutation catalog with the mut_mat() function and the relative contribution plot was extracted with plot_96_profile(). The COSMIC version 3 signatures were used and identified on the basis of a cosine similarity > 0.85.

Variant allele frequency calculations

The variant allele frequency (VAF) is a metric (range 0–1) that describes the fraction of reads covering a particular variant position and how much the coverage supports it. VAFs are expected to be around ~0.5 because a heterozygous mutation means that only one of the two alleles is altered, whereas a VAF of 0 shows no support in a variant and a VAF close to 1 shows that all reads support that variant. We plotted the VAF distribution for each clone including all variants (Extended Data Figs. 2, 5 and 6). A VAF filtering threshold of 0.3 was applied to discard mutations that were introduced after the single-cell sort according to a previous method[63].

Evaluation of MSI

We performed the comparison of two bioinformatics tools to calculate MSI: MANTIS[45] and MSMuTect version 2 (ref. 46). Both tools use

normal-tumor-paired, aligned and processed BAM files (hg19). The WGS clone CJMLH1C1 was used as normal. For MANTIS, we used the recommended settings for whole-exome usage (--mrq = 20.0 --mlq = 25.0 --mlc = 20 --mrr = 1) with a WES locus hg19 panel in BED format (included in the MANTIS repository). To run MSMutect2, we created a reference hg19 locus table with Phobos (version 3.3.12; http://www.rub.de/eco-evo/cm/cm_phobos.htm) with the same WES locus panel from MANTIS. We compared our clone or organoids to TCGA-COAD (MSI-H, MSS and MSMutect2). In the case of MANTIS, we recommend the use of the stepwise difference metric where any value greater 0.4 is considered MS-unstable (Fig. 4a).

Relative risk analysis

The relative mutation probability of driver gene mutations was calculated as described in the previous report[51]. Frequent mutations of MSI-H cancers in the Ras, Raf, MAPK, PI3K and ErbB pathways were selected from a previous study[50]. Mutational signatures in in vivo colonic and small intestinal tissue mutational signatures and in vitro colonic and small intestinal organoids were taken from our previous work[17,49].

Simultaneous inhibition of all four major pathways in vitro

Gene expression and protein analyses were prepared as follows. Organoids were passaged to single cells following an enzymatic dissociation with TrypLE for 10 min at 37 °C. Cells were then resuspended in Matrigel and cultured in full human colon organoid expansion medium for 5 days to allow organoid formation. Fully formed organoids were then washed three times in PBS and cultured for 24 h in either full expansion medium or selection medium (−WRNE + 1 mM Nut3, 1 µM Afa, 50 ng ml^{-1} BMP2 and 200 ng ml^{-1} DKK1). After 24 h, the organoids were collected and subjected to either RNA or protein extraction and used for RT–qPCR and western blot analyses.

RNA isolation, complementary DNA preparation and RT–qPCR

Organoids were collected in RLT lysis buffer supplemented with BME and mRNA was isolated using the QIAGEN RNeasy micro kit (QIAGEN) following the manufacturer's instructions. Following isolation, 1 µg of RNA was used for cDNA synthesis using GoScript reverse transcriptase (Promega) following the manufacturer's instructions. RT–qPCR was performed for a selection of genes using IQ SYBR green mix (Bio-Rad). Results were quantified using the $\Delta\Delta C_t$ method. All primer sequences are listed in Supplementary Table 4.

Western blotting

Cells were lysed in radioimmunoprecipitation assay buffer containing cOmplete EDTA-free protease inhibitor cocktail tablets (4693132001, Sigma-Aldrich). Protein quantification was performed using a standard Bradford assay (Bio-Rad) and equal amounts of protein were run on SDS–PAGE gels and transferred to PVDF membranes (Millipore). After transfer, membranes were blocked, washed and incubated with antibodies against p53 (1:1,000; DO-1, Santa Cruz Biotechnology), p21 (1:1,000; F-5, Santa Cruz Biotechnology), glyceraldehyde 3-phosphate dehydrogenase (GAPDH; 1:5,000; ab9485, Abcam), phospho-p44/42 MAPK (ERK1 and ERK2) (Thr202, Tyr204) (1:1,000; CST9101, Cell Signaling Technology) and β-actin (1:5,000; 13E5, Cell Signaling Technology). The signals were detected using enhanced chemiluminescence (SuperSignal West Femto maximum sensitivity substrate, Thermo Fisher Scientific).

Drug screening

Drug screenings were performed as described elsewhere[66]. In brief, outgrowing organoids were recovered from BME and enzymatically dissociated in TrypLE for 5 min at 37 °C. Following TrypLE inactivation, dissociated organoids were resuspended in BME and allowed to recover for 2 days in a medium containing a low concentration of EGF (0.5 ng ml^{-1} before being cultured in a medium lacking EGF for two additional days. On the day of dispense, prewarmed dispase was added and the organoids were incubated for 1 h at 37 °C, after which the organoids were collected and washed with ice-cold AdDMF+++. The organoids were counted and dispensed at a density of 1,000 organoids per well in 40 µl of culture medium lacking EGF and containing 5% (v/v) BME using a multidrop dispenser (Thermo Fisher Scientific) in a 384-well plate. The inhibitors and the vehicle for the normalization were added with an HP D300e digital dispenser (Hewlett-Packard). After 5 days of treatment, 30 µl of Cell Titer Glo (Promega) was added to each well using a multidrop dispenser and the plate was shaken for 5 min and incubated for an additional 15 min at room temperature before the luminescence was read using a SPARK luminescence detector (Tecan) with Tecan SparkControl software (version 2.1). The experiments were performed on two different clones, each with three technical replicates; organoids before obtaining *NRAS* mutations were used as a control.

Generation of *KRAS*^{G12D} mutant organoid

Single guide RNAs (sgRNAs) targeting the human *KRAS* gene were cloned into an SpCas9–eGFP vector (Addgene, plasmid 48138) as previously described[67]. sgRNA and a homology-directed repair (HDR) donor DNA template for introducing the *KRAS*^{G12D} mutation were selected from the previous study[13]. To generate *KRAS*^{G12D} mutants, the organoids were dissociated into single cells with TrypLE express and transfected using a NEPA21 super electroporator (NEPA GENE) with SpCas9–eGFP containing the locus-specific sgRNA and the *KRAS*^{G12D} HDR template as described before[68]. Then, 3 days after transfection, culture medium supplemented with Y-27632 was exchanged with selection medium lacking EGF and containing 1 µM Gef (Selleck Chemicals) (−EGF+Gef). Clonal lines were generated by isolating individual organoids which survived the selection and dissociating them to single cells with TrypLE express. Outgrowing clones were separated and expanded as clonal lines that were used for subsequent analyses. Clonal lines were genotyped using the Zymogen Quick-DNA microprep kit following the manufacturer's instructions. Correct gene editing was verified by genomic DNA extraction followed by PCR amplification of targeted loci using Q5 high-fidelity polymerase (New England Biolabs). Finally, Sanger sequencing of the generated amplicons by Macrogen confirmed correct gene editing. Primers used for amplification and Sanger sequencing can be found in Supplementary Table 4.

In vivo subcutaneous transplantation

Clonal organoids were passaged with TrypLE Express (Thermo Fisher Scientific) and allowed to recover in the appropriate culture medium for 2 days before being collected for the transplantation. The cultured organoids were incubated with TrypLE Express in the presence of 10 µM Y-27632 (Tocris Bioscience) and mechanically dissociated into single cells and counted. A total of 200,000 cells were resuspended in 100 µl of culture medium, mixed with Cultrex BME (Trevigen) at a 1:1 ratio and subcutaneously injected into both sides of the posterior flank of NSG mice (n = 3–6 mice, 6–12 injection sites per organoid line) as previously described[13]. Then, 8 weeks after transplantation, the mice were killed and analyzed for the presence of a tumor mass. Three mice in the CRISPR-AKPS organoid transplantation condition were killed with the estimation of exceeded maximal tumor burden 7 weeks after transplantation. Tumor volume was calculated using the modified ellipsoidal formula ((length × width^2)/2)[69]. After measuring, the tumor specimens were fixed overnight at 4 °C in 4% PFA, paraffin-embedded and processed for histological analyses.

Histology

Tissues and organoids were fixed in 4% PFA, dehydrated in ethanol and embedded in paraffin. Sections were subjected to hematoxylin and eosin (H&E) and immunohistochemical (IHC) staining. Slides were cut at 5-µm thickness and used for histology. Organoids were stained

with H&E or primary antibodies for IHC. In brief, the organoids were dehydrated in an ethanol gradient and then rinsed in PBS. Heat-induced antigen retrieval was performed and the slides were sequentially incubated with the primary and secondary antibodies. Finally, DAB was applied on the slides, which were then counterstained with hematoxylin, dehydrated and mounted with permanent mounting medium. The imaging was performed on a LEICA microscope (DM6000) and images were processed using Leica LAS-X (version 1.1) software. The following primary antibodies were used for IHC staining: mouse anti-E-cadherin clone 36 (1:1,000; 610182, BD Biosciences), mouse anti-Ki67 clone MM1 (1:1,000; 550609, BD Pharmingen), rabbit anti-β-catenin H-102 (1:500; sc-7199, Santa Cruz Biotechnology) and rabbit anti-EGFR clone EP38Y (1:1,000; ab52894, Abcam).

Statistics and reproducibility

No statistical method was used to predetermine sample size but our sample sizes are similar to those reported in a previous publication[13]. No data were excluded from the analyses. The experiments were not randomized. The investigators were not blinded to allocation during experiments and outcome assessment. Data collection and analysis were not performed blind to the conditions of the experiments. Data distribution was assumed to be normal but this was not formally tested. Statistical analysis was performed with Prism 9.0 (GraphPad, Dotmatics). For comparisons between two independent groups, a two-tailed unpaired Welch's *t*-test was used. *P* values < 0.05 were defined as statistically significant.

Reporting summary

Further information on research design is available in the Nature Portfolio Reporting Summary linked to this article.

Data availability

The sequencing data were deposited to the European Genome–Phenome Archive (https://ega-archive.org/) under accession numbers EGAS00001001682, EGAS00001000881 and EGAS50000000114. All other data supporting the findings of this study are available from the corresponding authors upon request. Source data are provided with this paper.

Code availability

Mutation calling and filtering pipeline NF-IAP is available from GitHub (https://github.com/ToolsVanBox/NF-IAP). Somatic variants were extracted with SMuRF version 3.0.0 (available from GitHub: https://github.com/ToolsVanBox/SMuRF) and MutationalPatterns (available from GitHub: https://github.com/ToolsVanBox/MutationalPatterns). In-house R scripts (version 4.2.3) were used to generate VAF plots and the comparison of MANTIS and MSMutect2 with library ggplo2.

References

1. Keum, N. & Giovannucci, E. Global burden of colorectal cancer: emerging trends, risk factors and prevention strategies. *Nat. Rev. Gastroenterol. Hepatol.* **3**, 153–20 (2019).
2. Dunican, D. S., McWilliam, P., Tighe, O., Parle-McDermott, A. & Croke, D. T. Gene expression differences between the microsatellite instability (MIN) and chromosomal instability (CIN) phenotypes in colorectal cancer revealed by high-density cDNA array hybridization. *Oncogene* **21**, 3253–3257 (2002).
3. Muzny, D. M. et al. Comprehensive molecular characterization of human colon and rectal cancer. *Nature* **487**, 330–337 (2012).
4. Fearon, E. R. & Vogelstein, B. A genetic model for colorectal tumorigenesis. *Cell* **61**, 759–767 (1990).
5. Deng, G. et al. *BRAF* mutation is frequently present in sporadic colorectal cancer with methylated *hMLH1*, but not in hereditary nonpolyposis colorectal cancer. *Clin. Cancer Res.* **10**, 191–195 (2004).
6. Leggett, B. & Whitehall, V. Role of the serrated pathway in colorectal cancer pathogenesis. *Gastroenterology* **138**, 2088–2100 (2010).
7. Liu, W. et al. Mutations in *AXIN2* cause colorectal cancer with defective mismatch repair by activating β-catenin/TCF signalling. *Nat. Genet.* **26**, 146–147 (2000).
8. Shimizu, Y. et al. Frequent alterations in the Wnt signaling pathway in colorectal cancer with microsatellite instability. *Genes Chromosomes Cancer* **33**, 73–81 (2002).
9. Jin, L. H. et al. Detection of point mutations of the *AXIN1* gene in colorectal cancers. *Int. J. Cancer* **107**, 696–699 (2003).
10. Zaidi, S. H. et al. Landscape of somatic single nucleotide variants and indels in colorectal cancer and impact on survival. *Nat. Commun.* **11**, 3644 (2020).
11. Cortes-Ciriano, I., Lee, S., Park, W.-Y., Kim, T.-M. & Park, P. J. A molecular portrait of microsatellite instability across multiple cancers. *Nat. Commun.* **8**, 15180 (2017).
12. Jung, B. et al. Loss of activin receptor type 2 protein expression in microsatellite unstable colon cancers. *Gastroenterology* **126**, 654–659 (2004).
13. Drost, J. et al. Sequential cancer mutations in cultured human intestinal stem cells. *Nature* **521**, 43–47 (2015).
14. Matano, M. et al. Modeling colorectal cancer using CRISPR–Cas9-mediated engineering of human intestinal organoids. *Nat. Med.* **21**, 256–262 (2015).
15. Fumagalli, A. et al. Genetic dissection of colorectal cancer progression by orthotopic transplantation of engineered cancer organoids. *Proc. Natl Acad. Sci. USA* **114**, E2357–E2364 (2017).
16. Giannakis, M. et al. *RNF43* is frequently mutated in colorectal and endometrial cancers. *Nat. Genet.* **46**, 1264–1266 (2014).
17. Drost, J. et al. Use of CRISPR-modified human stem cell organoids to study the origin of mutational signatures in cancer. *Science* **358**, 234–238 (2017).
18. Boland, C. R. & Goel, A. Microsatellite Instability in Colorectal Cancer. *Gastroenterology* **138**, 2073–2087 (2010).
19. Bonadona, V. et al. Cancer risks associated with germline mutations in *MLH1, MSH2,* and *MSH6* genes in Lynch syndrome. *JAMA* **305**, 2304–2310 (2011).
20. Kane, M. F. et al. Methylation of the *hMLH1* promoter correlates with lack of expression of *hMLH1* in sporadic colon tumors and mismatch repair-defective human tumor cell lines. *Cancer Res.* **57**, 808–811 (1997).
21. Veigl, M. L. et al. Biallelic inactivation of *hMLH1* by epigenetic gene silencing, a novel mechanism causing human MSI cancers. *Proc. Natl Acad. Sci. USA* **95**, 8698–8702 (1998).
22. Geurts, M. H. et al. CRISPR-based adenine editors correct nonsense mutations in a cystic fibrosis organoid biobank. *Cell Stem Cell* **26**, 503–510.e7 (2020).
23. Schwank, G. et al. Functional repair of *CFTR* by CRISPR/Cas9 in intestinal stem cell organoids of cystic fibrosis patients. *Cell Stem Cell* **13**, 653–658 (2013).
24. Ringel, T. et al. Genome-scale CRISPR screening in human intestinal organoids identifies drivers of TGF-β resistance. *Cell Stem Cell* **26**, 431–440.e8 (2020).
25. Bugter, J. M., Fenderico, N. & Maurice, M. M. Mutations and mechanisms of Wnt pathway tumour suppressors in cancer. *Nat. Rev. Cancer* **21**, 5–21 (2021).
26. Mazzoni, S. M., Petty, E. M., Stoffel, E. M. & Fearon, E. R. An *AXIN2* mutant allele associated with predisposition to colorectal neoplasia has context-dependent effects on AXIN2 protein function. *Neoplasia* **17**, 463–472 (2015).
27. Thorvaldsen, T. E., Pedersen, N. M., Wenzel, E. M. & Stenmark, H. Differential Roles of AXIN1 and AXIN2 in tankyrase inhibitor-induced formation of degradasomes and β-catenin degradation. *PLoS ONE* **12**, e0170508 (2017).

28. Sanson, R. et al. *AXIN1* protects colon carcinogenesis by an immune-mediated effect. *Cell. Mol. Gastroenterol. Hepatol.* **15**, 689–715 (2023).
29. Alexandrov, L. B. et al. The repertoire of mutational signatures in human cancer. *Nature* **578**, 94–101 (2020).
30. Thorstensen, L. et al. Genetic and epigenetic changes of components affecting the Wnt pathway in colorectal carcinomas stratified by microsatellite instability. *Neoplasia* **7**, 99–108 (2005).
31. Lammi, L. et al. Mutations in *AXIN2* cause familial tooth agenesis and predispose to colorectal cancer. *Am. J. Hum. Genet.* **74**, 1043–1050 (2004).
32. Robles, A. I. et al. Whole-exome sequencing analyses of inflammatory bowel disease-associated colorectal cancers. *Gastroenterology* **150**, 931–943 (2016).
33. Chandran, S. S. et al. Immunogenicity and therapeutic targeting of a public neoantigen derived from mutated *PIK3CA*. *Nat. Med.* **28**, 946–957 (2022).
34. Kodach, L. L. et al. The bone morphogenetic protein pathway is inactivated in the majority of sporadic colorectal cancers. *Gastroenterology* **134**, 1332–1341 (2008).
35. Park, S. W., Hur, S. Y., Yoo, N. J. & Lee, S. H. Somatic frameshift mutations of bone morphogenic protein receptor 2 gene in gastric and colorectal cancers with microsatellite instability. *APMIS* **118**, 824–829 (2010).
36. Takeda, H. et al. CRISPR–Cas9-mediated gene knockout in intestinal tumor organoids provides functional validation for colorectal cancer driver genes. *Proc. Natl Acad. Sci. USA* **116**, 15635–15644 (2019).
37. Jung, B., Staudacher, J. J. & Beauchamp, D. Transforming growth factor β superfamily signaling in development of colorectal cancer. *Gastroenterology* **152**, 36–52 (2017).
38. Alexandrov, L. B. et al. Signatures of mutational processes in human cancer. *Nature* **500**, 415–421 (2013).
39. Post, J. B. et al. Cancer modeling in colorectal organoids reveals intrinsic differences between oncogenic *RAS* and *BRAF* variants. Preprint at *bioRxiv* https://doi.org/10.1101/860122 (2019).
40. Ponsioen, B. et al. Quantifying single-cell ERK dynamics in colorectal cancer organoids reveals EGFR as an amplifier of oncogenic MAPK pathway signalling. *Nat. Cell Biol.* **23**, 377–390 (2021).
41. Vaughn, C. P., ZoBell, S. D., Furtado, L. V., Baker, C. L. & Samowitz, W. S. Frequency of *KRAS*, *BRAF*, and *NRAS* mutations in colorectal cancer. *Genes Chromosomes Cancer* **50**, 307–312 (2011).
42. Serebriiskii, I. G. et al. Comprehensive characterization of *RAS* mutations in colon and rectal cancers in old and young patients. *Nat. Commun.* **10**, 3722 (2019).
43. Valencia-Sama, I. et al. *NRAS* status determines sensitivity to SHP2 inhibitor combination therapies targeting the Ras–MAPK pathway in neuroblastoma. *Cancer Res.* **80**, 3413–3423 (2020).
44. Gebregiworgis, T. et al. The Q61H mutation decouples KRAS from upstream regulation and renders cancer cells resistant to SHP2 inhibitors. *Nat. Commun.* **12**, 6274 (2021).
45. Kautto, E. A. et al. Performance evaluation for rapid detection of pan-cancer microsatellite instability with MANTIS. *Oncotarget* **8**, 7452–7463 (2016).
46. Maruvka, Y. E. et al. Analysis of somatic microsatellite indels identifies driver events in human tumors. *Nat. Biotechnol.* **35**, 951–959 (2017).
47. Walker, R. et al. Evaluating multiple next-generation sequencing-derived tumor features to accurately predict DNA mismatch repair status. *J. Mol. Diagn.* **25**, 94–109 (2023).
48. Hause, R. J., Pritchard, C. C., Shendure, J. & Salipante, S. J. Classification and characterization of microsatellite instability across 18 cancer types. *Nat. Med.* **22**, 1342–1350 (2016).
49. Blokzijl, F. et al. Tissue-specific mutation accumulation in human adult stem cells during life. *Nature* **538**, 260–264 (2016).
50. Kloth, M. et al. Activating *ERBB2/HER2* mutations indicate susceptibility to pan-HER inhibitors in Lynch and Lynch-like colorectal cancer. *Gut* **65**, 1296–1305 (2016).
51. Temko, D., Tomlinson, I. P. M., Severini, S., Schuster-Böckler, B. & Graham, T. A. The effects of mutational processes and selection on driver mutations across cancer types. *Nat. Commun.* **9**, 1857–10 (2018).
52. Domingo, E. et al. *BRAF* screening as a low-cost effective strategy for simplifying HNPCC genetic testing. *J. Med. Genet.* **41**, 664 (2004).
53. Caravagna, G. et al. Algorithmic methods to infer the evolutionary trajectories in cancer progression. *Proc. Natl Acad. Sci. USA* **113**, E4025–E4034 (2016).
54. Sato, T. et al. Long-term expansion of epithelial organoids from human colon, adenoma, adenocarcinoma, and Barrett's epithelium. *Gastroenterology* **141**, 1762–1772 (2011).
55. van de Wetering, M. et al. Prospective derivation of a living organoid biobank of colorectal cancer patients. *Cell* **161**, 933–945 (2015).
56. Roerink, S. F. et al. Intra-tumour diversification in colorectal cancer at the single-cell level. *Nature* **556**, 457–462 (2018).
57. Fujii, M. et al. A colorectal tumor organoid library demonstrates progressive loss of niche factor requirements during tumorigenesis. *Cell Stem Cell* **18**, 827–838 (2016).
58. Bohaumilitzky, L. et al. The different immune profiles of normal colonic mucosa in cancer-free Lynch syndrome carriers and Lynch syndrome colorectal cancer patients. *Gastroenterology* **162**, 907–919.e10 (2022).
59. Chang, K. et al. Immune profiling of premalignant lesions in patients with Lynch syndrome. *JAMA Oncol.* **4**, 1085 (2018).
60. Karlsson, K. et al. Deterministic evolution and stringent selection during preneoplasia. *Nature* **618**, 383–393 (2023).
61. Li, H. & Durbin, R. Fast and accurate long-read alignment with Burrows–Wheeler transform. *Bioinformatics* **26**, 589–595 (2010).
62. Bertrums, E. J. M. et al. Elevated mutational age in blood of children treated for cancer contributes to therapy-related myeloid neoplasms. *Cancer Discov.* **12**, OF1–OF14 (2022).
63. Jager, M. et al. Measuring mutation accumulation in single human adult stem cells by whole-genome sequencing of organoid cultures. *Nat. Protoc.* **13**, 59–78 (2018).
64. DePristo, M. A. et al. A framework for variation discovery and genotyping using next-generation DNA sequencing data. *Nat. Genet.* **43**, 491–498 (2011).
65. Blokzijl, F., Janssen, R., van Boxtel, R. & Cuppen, E. MutationalPatterns: comprehensive genome-wide analysis of mutational processes. *Genome Med.* **10**, 33 (2018).
66. Driehuis, E., Kretzschmar, K. & Clevers, H. Establishment of patient-derived cancer organoids for drug-screening applications. *Nat. Protoc.* **15**, 3380–3409 (2020).
67. Ran, F. A. et al. Genome engineering using the CRISPR–Cas9 system. *Nat. Protoc.* **8**, 2281–2308 (2013).
68. Fujii, M., Matano, M., Nanki, K. & Sato, T. Efficient genetic engineering of human intestinal organoids using electroporation. *Nat. Protoc.* **10**, 1474–1485 (2015).
69. Tomayko, M. M. & Reynolds, C. P. Determination of subcutaneous tumor size in athymic (nude) mice. *Cancer Chemother. Pharmacol.* **24**, 148–154 (1989).

Acknowledgements

We thank A. Brousali, J. Salij and O. Kranenburg of the Utrecht Platform for Organoid Technology (UMC Utrecht) for patient inclusion and tissue acquisition, S. van den Brink for Wnt3a-conditioned medium

and R-spondin 1-conditioned medium production and S. van der Elst for help with fluorescence-activated cell sorting. We also thank the members of the contributing labs for helpful suggestions and discussions. This work was supported by an award from the Cancer Research UK Grand Challenge (C6307/A29058), the Mark Foundation for Cancer Research to the SPECIFICANCER team, the 'Sta op tegen Kanker (Stand Up To Cancer)' International Translational Cancer Research grant to T.M. and H.C. and Oncode Accelerator, a Dutch National Growth Fund project under grant number NGFOP22201 (Organoid Group). M.B. is a postdoctoral fellow supported by a long-term EMBO fellowship (ALTF 765-2019). R.v.B. is a New York Stem Cell Foundation Robertson Investigator and is supported by The New York Stem Cell Foundation.

Author contributions

T.M., J.D. and H.C. conceptualized and designed the project. T.M. and M.B. performed major experiments and analyzed the data. S.L. performed the organoid culture and western blotting experiments. M.H.G. assisted with CRISPR–Cas9 genome editing. H.B. and J.K. performed the IHC staining. J.K. and J.H.v.E. performed the transplantation experiments. D.M.G., R.O. and R.v.B. performed the WGS data analyses. T.M., M.B. and H.C. wrote the paper. H.C. supervised the study. All authors discussed the results and commented on the manuscript.

Competing interests

H.C. is the inventor of several patents related to organoid technology; his full disclosure is given at https://www.uu.nl/staff/JCClevers/. The other authors declare no competing interests.

Additional information

Extended data is available for this paper at https://doi.org/10.1038/s43018-024-00841-x.

Supplementary information The online version contains supplementary material available at https://doi.org/10.1038/s43018-024-00841-x.

Correspondence and requests for materials should be addressed to Hans Clevers.

Peer review information *Nature Cancer* thanks Senthil Muthuswamy, Eduardo Vilar and Omer Yilmaz for their contribution to the peer review of this work.

Reprints and permissions information is available at www.nature.com/reprints.

Publisher's note Springer Nature remains neutral with regard to jurisdictional claims in published maps and institutional affiliations.

[1]Hubrecht Institute, Royal Netherlands Academy of Arts and Sciences (KNAW) and UMC Utrecht, Utrecht, The Netherlands. [2]Oncode Institute, Utrecht, The Netherlands. [3]The Princess Máxima Center for Pediatric Oncology, Utrecht, The Netherlands. [4]Present address: Department of Gastroenterology and Hepatology, Institute of Science Tokyo, Tokyo, Japan. [5]Present address: Roche Pharmaceutical Research and Early Development, Basel, Switzerland. [6]These authors contributed equally: Tomohiro Mizutani, Matteo Boretto. ✉e-mail: h.clevers@hubrecht.eu

https://doi.org/10.1038/s43018-024-00841-x

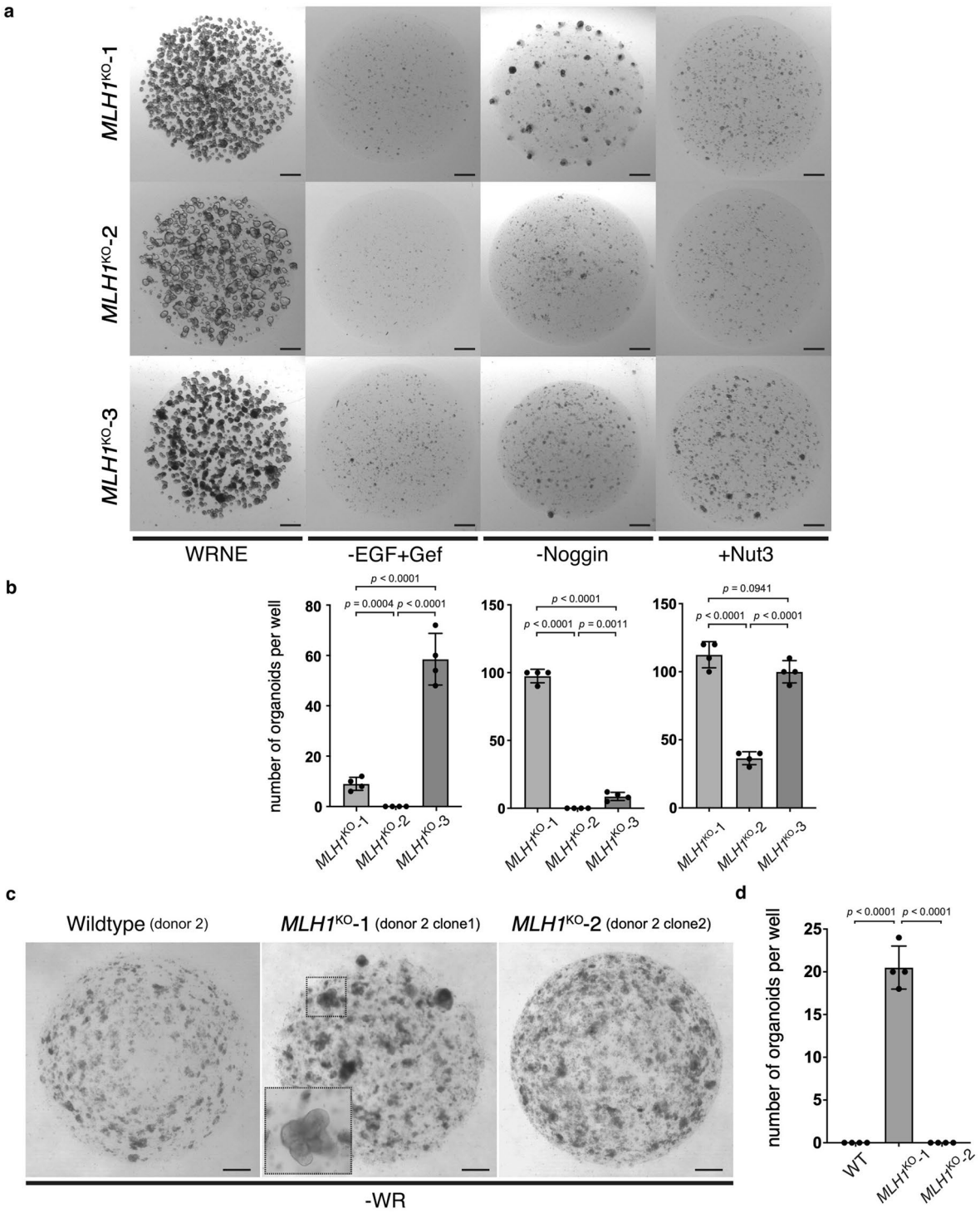

Extended Data Fig. 1 | Various niche factor selection of *MLH1*^{KO} human colon organoids. (**a**) MLH1^{KO}-1 organoids were selected by inhibition of other niche factor pathways. Triple independent *MLH1*^{KO}-1 organoid lines grew in complete medium (WRNE), but all of small organoids formed in all conditions died within a week (representative pictures from $n = 3$ clonal organoid lines). W, wnt3a; R, R-spondin1; N, Noggin; E, EGF; Gef, gefitinib. Scale bars, 500 µm. (**b**) Quantification of formed organoids in each condition. Mean and SD (error bars) of $n = 4$ clonal organoid lines. -EGF+Gef ($P = 0.0004$, $P < 0.0001$, $P < 0.0001$), -Noggin ($P < 0.0001$, $P = 0.0011$, $P < 0.0001$), +Nut3 ($P < 0.0001$, $P < 0.0001$, $P = 0.0941$), two-sided Welch's t-test. (**c**) MLH1^{KO}-1 organoid clones established from another individual were selected with the deprivation of Wnt factor. Some of organoids grew out only from MLH1^{KO}-1 clone in -WR medium. Outgrowing clones are shown in inset. Scale bars, 500 µm. (**d**) Quantification of survived organoids in each condition. Mean and SD (error bars) of $n = 4$ clonal organoid lines. $P < 0.0001$, $P < 0.0001$, two-sided Welch's t-test.

https://doi.org/10.1038/s43018-024-00841-x

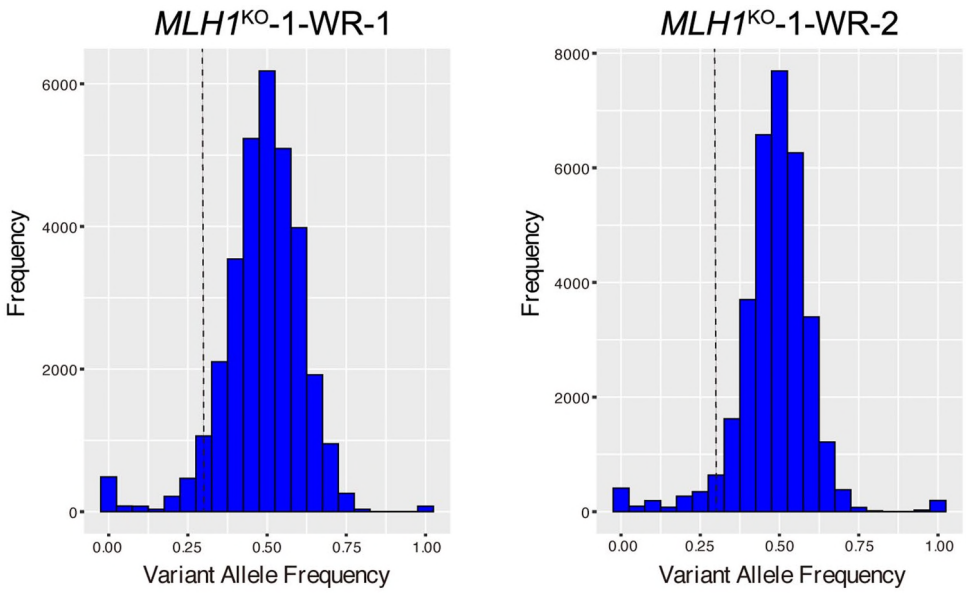

Extended Data Fig. 2 | Variant Allele Frequency distribution of mutant clones. Graphs show Variant Allele Frequency (VAF) distribution of somatic mutations per organoid clone (*MLH1*^{KO}-1-WR-1 and *MLH1*^{KO}-1-WR-2) in WGS. A VAF-filtering threshold of 0.3 (dotted line) is applied to discard mutations that are introduced after the single-cell sort.

https://doi.org/10.1038/s43018-024-00841-x

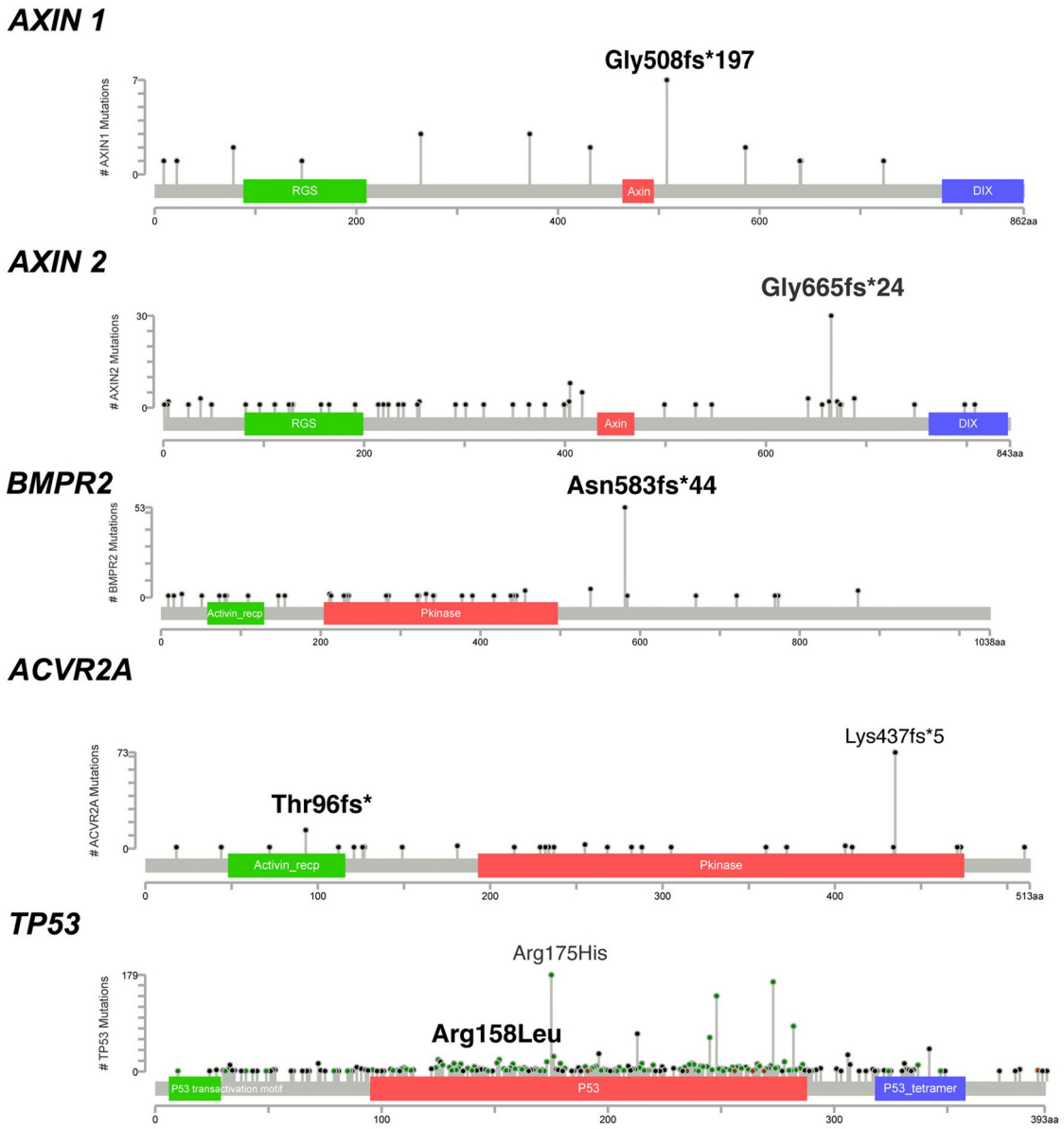

Extended Data Fig. 3 | Mutational spectrum of *AXIN1*, *AXIN2*, *BMPR2*, *ACVR2A*, and *TP53* in CRC. Lollipop diagram corresponding colorectal cancer studies selected in cBioPortal (https://www.cbioportal.org). A black dot indicated a truncating mutation; a green dot indicated a missense mutation; and a purple dot indicated other types of mutation. The length of each lollipop represents the number of patients with the specific mutation. Specific mutations found in *MLH1*^{KO}-1 organoid are represented on top of each lollipop.

https://doi.org/10.1038/s43018-024-00841-x

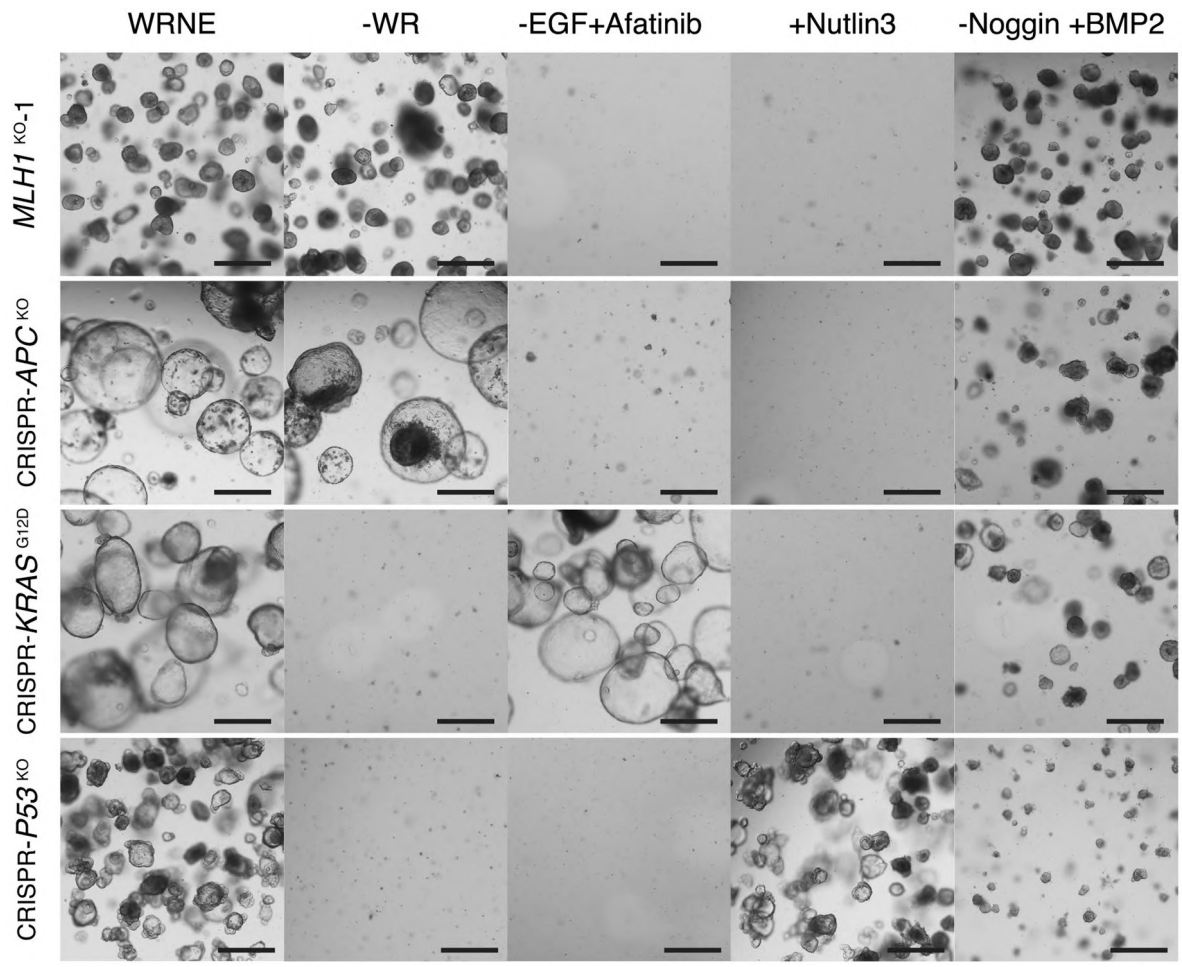

Extended Data Fig. 4 | *MLH1*^{KO} *AXIN1/2*-mutant organoids only gained Wnt-pathway independency. The medium selection experiments with the *MLH1*^{KO} *AXIN1/2*-mutant organoids (*MLH1*^{KO}-1) and each pathway driver CRISPR-mutant organoids (CRISPR-*APC*^{KO}, CRISPR-*KRAS*^{G12D}, CRISPR-*P53*^{KO}) in WRNE (complete medium), -WR, -EGF +Afatinib, +Nutulin3, and -Noggin+BMP2. Representative pictures from $n = 3$ clonal organoid lines. Scale bars, 200 µm.

https://doi.org/10.1038/s43018-024-00841-x

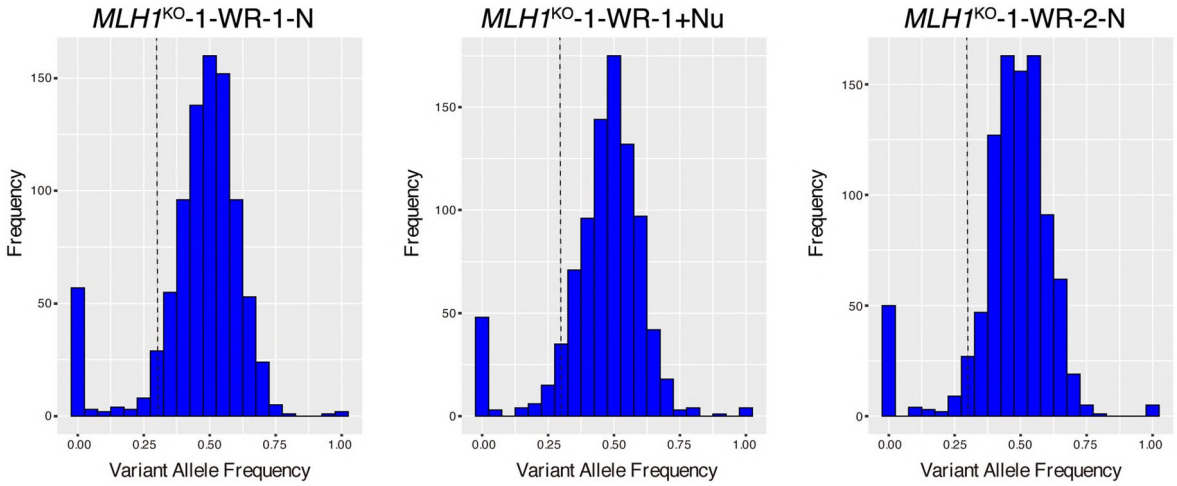

Extended Data Fig. 5 | Variant Allele Frequency distribution of mutant clones. Graphs show Variant Allele Frequency (VAF) distribution of somatic mutations per organoid clone (*MLH1*^{KO}-1-WR-1-N, *MLH1*^{KO}-1-WR-1+Nu, and *MLH1*^{KO}-1-WR-2-N) in WES. A VAF-filtering threshold of 0.3 (dotted line) is applied to discard mutations that are introduced after the single-cell sort.

https://doi.org/10.1038/s43018-024-00841-x

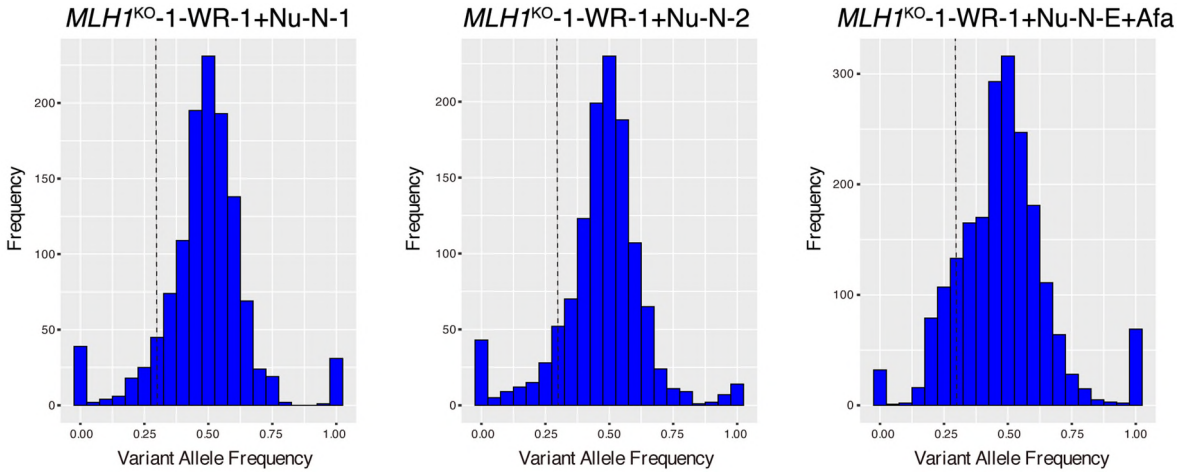

Extended Data Fig. 6 | Variant Allele Frequency distribution of mutant clones. Graphs show Variant Allele Frequency (VAF) distribution of somatic mutations per organoid clone (*MLH1*^{KO}-1-WR-1+Nu-N-1, *MLH1*^{KO}-1-WR-1+Nu-N-2, and *MLH1*^{KO}-1-WR-1+Nu-N-E+Afa) in WES. A VAF-filtering threshold of 0.3 (dotted line) is applied to discard mutations that are introduced after the single-cell sort.

https://doi.org/10.1038/s43018-024-00841-x

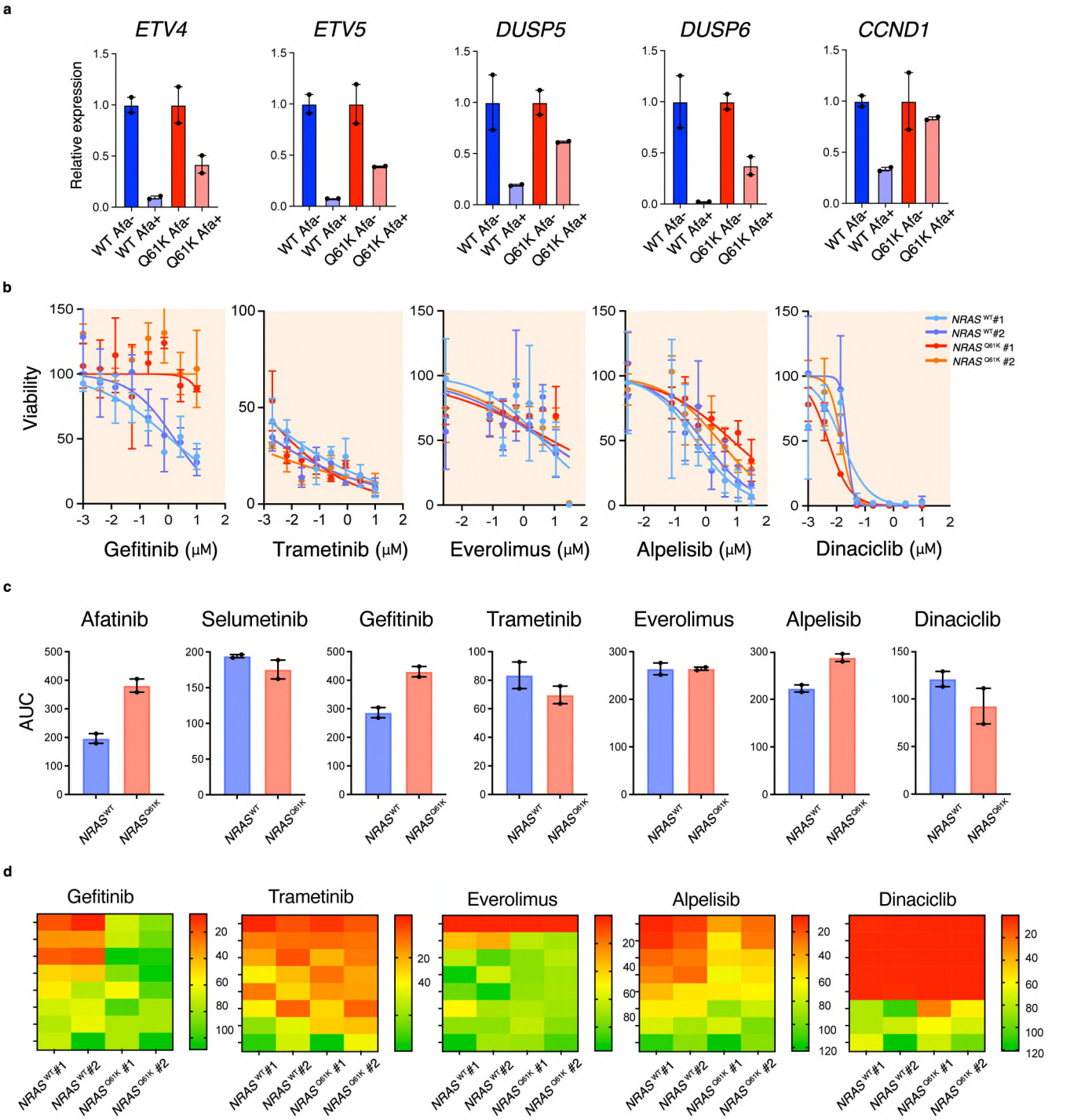

Extended Data Fig. 7 | Drug sensitivity assay of *NRAS*^{Q61K} mutant organoids. (**a**) qRT-PCR analysis of *ETV4*, *ETV5*, *DUSP4*, *DUSP5* and *CCND1* mRNA levels. These transcripts were compared between *NRAS* wildtype parental clone (WT) and NRAS-Q61K clone cultured in the medium with or without afatinib (Afa+/-). $n = 2$ clonal organoid lines. (**b**) Dose-response curves showing the sensitivity of NRAS-WT and NRAS-Q61K clones to inhibitors of the EGFR (Gefitinib), MEK (Trametinib), mTOR/PI3Kα (Everolimus/Alpelisib) and CDKs (Dinaciclib). Y-axis represent the viability of the samples while X-axis represent the drug concentration (power of 10 μM). Mean and SD (error bars) of $n = 3$ technical replicates for $n = 2$ independent organoid clones for each genetic background. (**c**) Representative bar graphs showing the sensitivity of NRAS-WT and NRAS-Q61K organoids to different inhibitors, calculated as area under the curve (AUC). $n = 2$ clonal organoid lines. (**d**) Heatmaps reporting the viability of the drug screening performed on NRAS-WT and NRAS-Q61K organoids as normalized to vehicle treated organoids. Color mapping range from low viability (red) to high viability (green).

https://doi.org/10.1038/s43018-024-00841-x

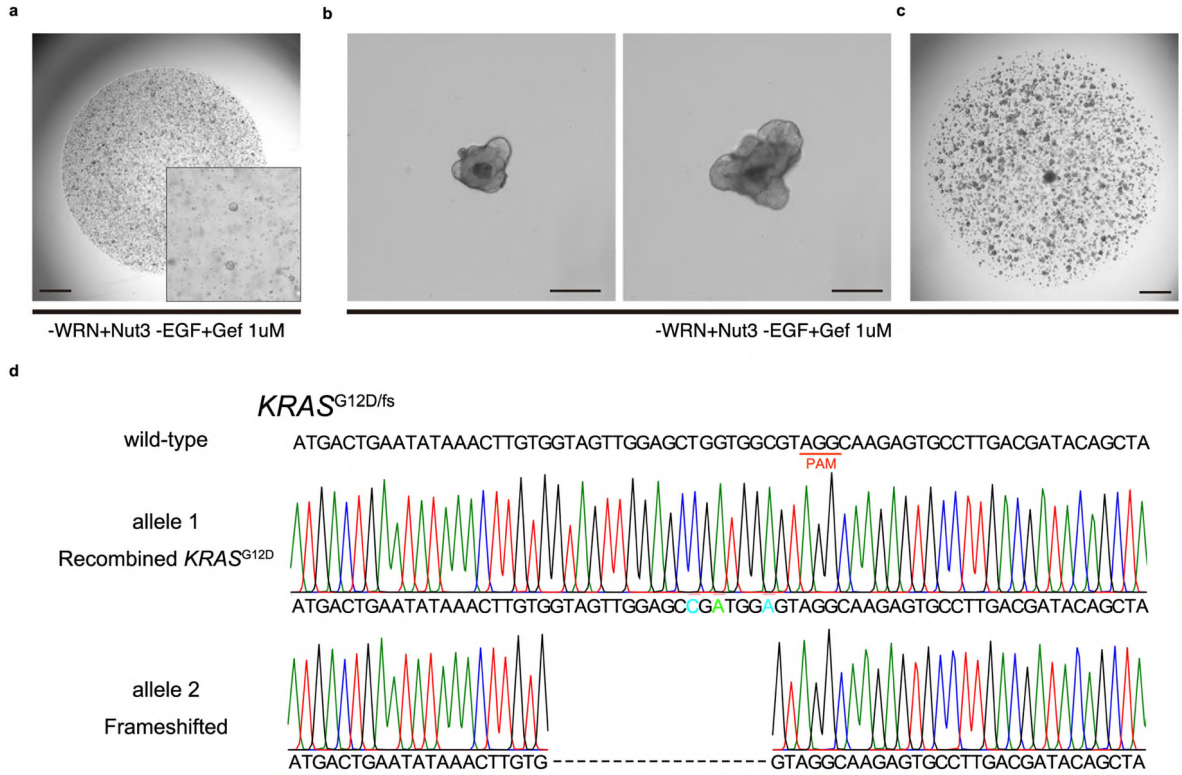

Extended Data Fig. 8 | Introduction of *KRAS*^{G12D} mutation on triple-pathway mutant organoids. (**a**) Triple-pathway mutant organoids were transfected with Cas9, sgRNA and the oligonucleotide previously designed for *KRAS*^{G12D} mutation. *KRAS*^{G12D} mutants were selected in the medium lacking EGF, with the EGFR inhibitor gefitinib (-WRNE+Nut3+Gef). Small single organoids survived and grew (Inset). Representative pictures from $n = 3$ clonal organoid lines. Scale bars, 500 µm. (**b**) Picked up surviving *KRAS*^{G12D} mutant organoid (representative pictures from $n = 3$ clonal organoid lines). Scale bars, 100 µm. (**c**) Single survived organoids were expanded and passaged in the medium lacking EGF, with the EGFR inhibitor gefitinib (-WRNE+Nut3+Gef). Representative pictures from $n = 3$ independent replicates. Scale bars, 500 µm. (**d**) Sequence analysis of the targeted *KRAS* exon. Oncogenic GGT > GAT mutation is indicated in green; silent mutations are in blue; protospacer adjacent motif (PAM) is underlined in red.

https://doi.org/10.1038/s43018-024-00841-x

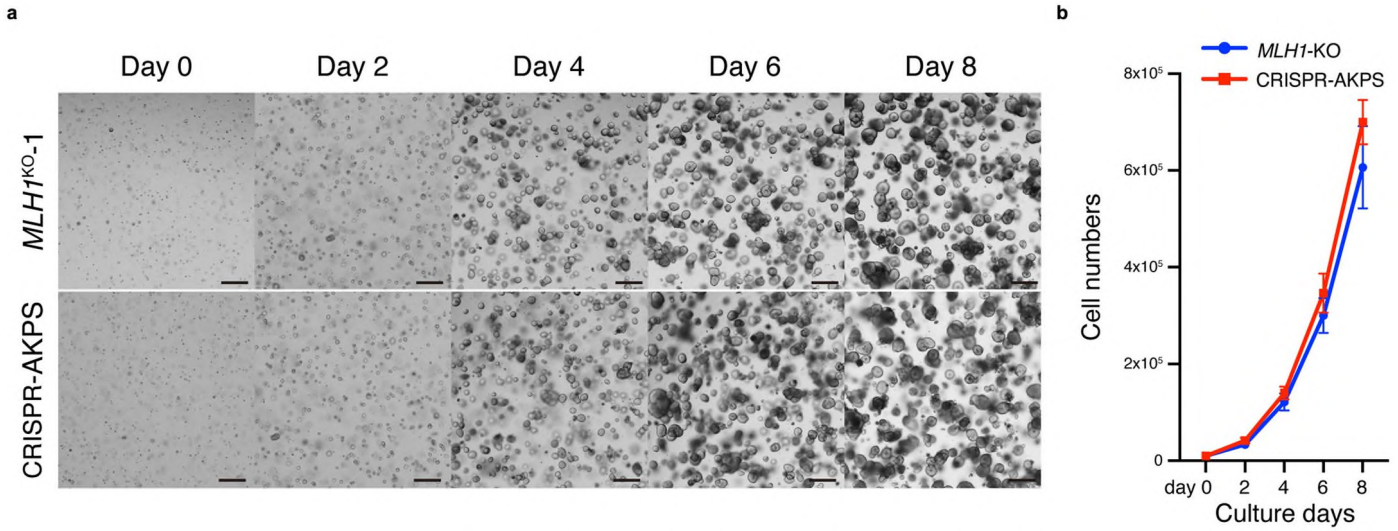

Extended Data Fig. 9 | Growth speed of AKPS mutant organoids and the quadruple-pathway mutant organoids. (**a**) the quadruple-pathway mutant organoids (*NRAS*^{Q61K}) and AKPS mutant organoids grew in complete medium (WRNE). Representative pictures from $n = 3$ clonal organoid lines. Scale bars, 100 µm. (**b**) Quantification in cell numbers of the quadruple-pathway mutant organoids (*NRAS*^{Q61K}) and AKPS mutant organoids Mean and SD (error bars) of $n = 3$ clonal organoid lines.

nature portfolio

Corresponding author(s): Hans Clevers

Last updated by author(s): Sep 16, 2024

Reporting Summary

Nature Portfolio wishes to improve the reproducibility of the work that we publish. This form provides structure for consistency and transparency in reporting. For further information on Nature Portfolio policies, see our Editorial Policies and the Editorial Policy Checklist.

Statistics

For all statistical analyses, confirm that the following items are present in the figure legend, table legend, main text, or Methods section.

n/a	Confirmed	
☐	☒	The exact sample size (*n*) for each experimental group/condition, given as a discrete number and unit of measurement
☐	☒	A statement on whether measurements were taken from distinct samples or whether the same sample was measured repeatedly
☐	☒	The statistical test(s) used AND whether they are one- or two-sided *Only common tests should be described solely by name; describe more complex techniques in the Methods section.*
☐	☒	A description of all covariates tested
☐	☒	A description of any assumptions or corrections, such as tests of normality and adjustment for multiple comparisons
☐	☒	A full description of the statistical parameters including central tendency (e.g. means) or other basic estimates (e.g. regression coefficient) AND variation (e.g. standard deviation) or associated estimates of uncertainty (e.g. confidence intervals)
☐	☒	For null hypothesis testing, the test statistic (e.g. *F*, *t*, *r*) with confidence intervals, effect sizes, degrees of freedom and *P* value noted *Give P values as exact values whenever suitable.*
☒	☐	For Bayesian analysis, information on the choice of priors and Markov chain Monte Carlo settings
☒	☐	For hierarchical and complex designs, identification of the appropriate level for tests and full reporting of outcomes
☒	☐	Estimates of effect sizes (e.g. Cohen's *d*, Pearson's *r*), indicating how they were calculated

Our web collection on statistics for biologists contains articles on many of the points above.

Software and code

Policy information about availability of computer code

Data collection	Leica LAS X (v1.1), Tecan SparkControl software (v2.1).
Data analysis	Leica LAS X (v1.1), Tecan SparkControl software (v2.1), GraphPad PRISM (v9.0), R Studio (v1.2.1335), R (v4.2.3), Burrows-Wheeler Aligner mapping tool (v0.7.17), and GATK (v4.13.0). Mutation calling and filtering pipelines are available at https://github.com/UMCUGenetics/IAP, https://github.com/UMCUGenetics/SNVFI and https://github.com/ToolsVanBox/INDELFI, smMIP analysis script is available at https://github.com/ToolsVanBox/smMIPfil. MutationalPatterns at https://github.com/ToolsVanBox/MutationalPatterns.

For manuscripts utilizing custom algorithms or software that are central to the research but not yet described in published literature, software must be made available to editors and reviewers. We strongly encourage code deposition in a community repository (e.g. GitHub). See the Nature Portfolio guidelines for submitting code & software for further information.

Data

Policy information about availability of data

All manuscripts must include a data availability statement. This statement should provide the following information, where applicable:

- Accession codes, unique identifiers, or web links for publicly available datasets
- A description of any restrictions on data availability
- For clinical datasets or third party data, please ensure that the statement adheres to our policy

Data availability statement in the manuscript as follows: "The sequencing data have been deposited to the European Genome-Phenome Archive (https://ega-archive.org/) under accession numbers EGAS00001001682, EGAS00001000881 and EGAS50000000114. Source data for Figs. 1-5 and Extended Data Figs. 1-9 have been provided as Source Data files. All other data supporting the findings of this study are available from the corresponding authors upon request."

Research involving human participants, their data, or biological material

Policy information about studies with human participants or human data. See also policy information about sex, gender (identity/presentation), and sexual orientation and race, ethnicity and racism.

Reporting on sex and gender	Mutated colon organoids were established from two wild-type human colon organoid cultures in previous study. These were derived from endoscopy material of a healthy donor (female, age 31 years) and from normal tissue of a resected colon segment derived from a patient (female, age 60 years) diagnosed with CRC (sigmoid). As the differences by sex in mutational progression were not expected, we did not consider sex or gender in our study design.
Reporting on race, ethnicity, or other socially relevant groupings	Ethnicity was not assessed.
Population characteristics	Mutated colon organoids were established from two wild-type human colon organoid cultures in previous study. These were derived from endoscopy material of a healthy donor (female, age 31 years) and from normal tissue of a resected colon segment derived from a patient (female, age 60 years) diagnosed with CRC (sigmoid).
Recruitment	Biopsy specimens for organoid cultures were obtained from the patients listed above.
Ethics oversight	The study was approved by the UMC Utrecht and Diakonessenhuis (Utrecht, Netherlands) ethical committee (TC-Bio 12-093) and was in accordance with the Declaration of Helsinki and according to Dutch law. This study is compliant with all relevant ethical regulations regarding research involving human participants.

Note that full information on the approval of the study protocol must also be provided in the manuscript.

Field-specific reporting

Please select the one below that is the best fit for your research. If you are not sure, read the appropriate sections before making your selection.

☒ Life sciences ☐ Behavioural & social sciences ☐ Ecological, evolutionary & environmental sciences

For a reference copy of the document with all sections, see nature.com/documents/nr-reporting-summary-flat.pdf

Life sciences study design

All studies must disclose on these points even when the disclosure is negative.

Sample size	No statistical method was used to predetermine sample size. We confirmed in vivo organoid transplantation results using multiple mice (3-6 mice per organoid line) according to previous experience(Drost et al. Nature 2015). For most in vitro experiments, we used n=>3 for according to previous experience with similar experiments. The sample size typically results in standard error <25% of the mean.
Data exclusions	No data from in vitro experiments were excluded. For in vivo experiments, animals were excluded only if they died or had to be killed according to protocols approved by the animal welfare committee.
Replication	Replicates for each experiment are described in the figure legends and methods. If not specified, the experiments were performed once with the presented number of data points shown in the figures. All datapoints were distinct; no repeated measures were used.
Randomization	For in vivo experiments of subcutaneous transplantation, animals were randomized. For in vitro experiments, all samples were analyzed equally with no sub-sampling therefore there was no requirement for randomization.
Blinding	Data collection and analyses were not performed blinded to the conditions of the experiments. For in vivo experiments, blinding was not performed because identification of mice was required due to practical constraints. For in vitro studies, experiments were not performed in a blinded manner because investigator need it to identify samples to perform treatments.

Reporting for specific materials, systems and methods

We require information from authors about some types of materials, experimental systems and methods used in many studies. Here, indicate whether each material, system or method listed is relevant to your study. If you are not sure if a list item applies to your research, read the appropriate section before selecting a response.

Materials & experimental systems

n/a	Involved in the study
☐	☒ Antibodies
☒	☐ Eukaryotic cell lines
☒	☐ Palaeontology and archaeology
☐	☒ Animals and other organisms
☒	☐ Clinical data
☒	☐ Dual use research of concern
☒	☐ Plants

Methods

n/a	Involved in the study
☒	☐ ChIP-seq
☒	☐ Flow cytometry
☒	☐ MRI-based neuroimaging

Antibodies

Antibodies used

Western blot analysis:
Mouse anti-P53 (clone DO-1), diluted 1:1000 (Santa Cruz Biotechnology, #sc-126)
Mouse anti-P21 (clone F-5), diluted 1:1000 (Santa Cruz Biotechnology, # sc-6246)
Rabbit anti-Phospho-p44/42 MAPK (Erk1/2) (Thr202/Tyr204), diluted 1:1000 (Cell Signaling Technology, CST9101)
Rabbit anti-β-Actin (13E5), diluted 1:5000 (Cell Signaling Technology, #4970)
Rabbit anti-GAPDH, diluted 1:5000 (Abcam, #ab-9485)

Immunohistochemistry:
Mouse anti-E-cadherin (clone 36), diluted 1:1000 (BD Biosciences, #610182)
Mouse anti-Ki67 (clone MM1), diluted 1:1000 (BD Pharmingen, #550609)
Rabbit anti-β-catenin (H-102), diluted 1:500 (Santa Cruz Biotechnology, #sc-7199)
Rabbit anti-EGFR (clone EP38Y), diluted 1:1000 (Abcam, #ab52894)

Validation

Antibodies used for western blot and immunohistochemistry have been validated on supplier's website and used in previous studies as cited below.

Western blot analysis:
Mouse anti-P53 (clone DO-1), diluted 1:1000 (Santa Cruz Biotechnology, #sc-126)
https://www.scbt.com/p/p53-antibody-do-1
Ref: Nature 521, 43–47 2015. https://doi.org/10.1038/nature14415
Mouse anti-P21 (clone F-5), diluted 1:1000 (Santa Cruz Biotechnology, # sc-6246)
https://www.scbt.com/p/p21-antibody-f-5
Ref: Nature 521, 43–47 2015. https://doi.org/10.1038/nature14415
Rabbit anti-Phospho-p44/42 MAPK (Erk1/2) (Thr202/Tyr204), diluted 1:1000 (Cell Signaling Technology, CST9101)
https://www.cellsignal.jp/products/primary-antibodies/phospho-p44-42-mapk-erk1-2-thr202-tyr204-antibody/9101
Ref: Nat Commun 12, 2656 2021. https://doi.org/10.1038/s41467-021-22969-5
Rabbit anti-β-Actin (13E5), diluted 1:5000 (Cell Signaling Technology, #4970)
https://www.cellsignal.com/products/primary-antibodies/b-actin-13e5-rabbit-mab/4970?producttype=siRNA%7CPolyclonal+Antibody&tab=product&Nrpp=100&No=100&fromPage=plp&language=en
Ref: PNAS 121 (12) e2309902121 2024. https://doi.org/10.1073/pnas.2309902121
Rabbit anti-GAPDH, diluted 1:5000 (Abcam, #ab-9485)
https://www.abcam.com/products/primary-antibodies/gapdh-antibody-loading-control-ab9485.html
Ref: Nature 521, 43–47 2015. https://doi.org/10.1038/nature14415

Immunohistochemistry:
Mouse anti-E-cadherin (clone 36), diluted 1:1000 (BD Biosciences, #610182)
https://www.bdbiosciences.com/en-us/products/reagents/microscopy-imaging-reagents/immunofluorescence-reagents/purified-mouse-anti-e-cadherin.610182
Ref: Nature 521, 43–47 2015. https://doi.org/10.1038/nature14415
Mouse anti-Ki67 (clone MM1), diluted 1:1000 (BD Pharmingen, #550609)
https://www.bdbiosciences.com/en-us/products/reagents/flow-cytometry-reagents/research-reagents/single-color-antibodies-ruo/purified-mouse-anti-ki-67.550609
Ref: Nature 521, 43–47 2015. https://doi.org/10.1038/nature14415
Rabbit anti-β-catenin (H-102), diluted 1:500 (Santa Cruz Biotechnology, #sc-7199)
https://www.scbt.com/p/beta-catenin-antibody-h-102
Rabbit anti-EGFR (clone EP38Y), diluted 1:1000 (Abcam, #ab52894)
Ref: PNAS 121 (12) e2309902121 2024. https://doi.org/10.1073/pnas.2309902121
https://www.abcam.com/products/primary-antibodies/egfr-antibody-ep38y-ab52894.html

Animals and other research organisms

Policy information about studies involving animals; ARRIVE guidelines recommended for reporting animal research, and Sex and Gender in Research

Laboratory animals	For mice experiments, 8-week-old NOD scid gamma (NSG; NOD.Cg-Prkdcscid Il2rgtm1Wjl/SzJ) mice were used in the study. The mice were kept in a constant temperature environment of 21°C (40–60% humidity) with a natural day/night light cycle in a conventional animal colony with free access to food and water. All the mice were housed in a pathogen-free vivarium in sterile, disposable microisolator cages and fed a sterile, irradiated diet with free access to sterile, irradiated water.
Wild animals	The study did not involve wild animals.
Reporting on sex	The performed experiment has no special request for the sex of animal models.
Field-collected samples	No field collected samples were used in the study.
Ethics oversight	All mouse experiments were conducted under a project license (AVD 8010020209924) granted by the Central Committee Animal Experimentation (CCD) of the Dutch government and approved by the KNAW-Hubrecht Institute Animal Welfare Body (IvD) (HI 21.39.04). All the mice were monitored and weighed once a week. Mice with symptoms of severe discomfort (e.g., >20 % weight loss compared to beginning, >15 % weight loss in two days) with tumor burden or with measured tumors larger than 1,000mm3 were humanely sacrificed. In this study, three mice in subcutaneous transplantation experiment were sacrificed with the estimation of exceeded maximal tumor burden in earlier time point. As tumor size was weekly checked by manual palpation, it was only possible to estimate the size of the tumors ahead of sacrifice. Indeed, we noted n = 1 tumor of the sacrificed animals exceeded the size limit.

Note that full information on the approval of the study protocol must also be provided in the manuscript.

Plants

Seed stocks	*Report on the source of all seed stocks or other plant material used. If applicable, state the seed stock centre and catalogue number. If plant specimens were collected from the field, describe the collection location, date and sampling procedures.*
Novel plant genotypes	*Describe the methods by which all novel plant genotypes were produced. This includes those generated by transgenic approaches, gene editing, chemical/radiation-based mutagenesis and hybridization. For transgenic lines, describe the transformation method, the number of independent lines analyzed and the generation upon which experiments were performed. For gene-edited lines, describe the editor used, the endogenous sequence targeted for editing, the targeting guide RNA sequence (if applicable) and how the editor was applied.*
Authentication	*Describe any authentication procedures for each seed stock used or novel genotype generated. Describe any experiments used to assess the effect of a mutation and, where applicable, how potential secondary effects (e.g. second site T-DNA insertions, mosiacism, off-target gene editing) were examined.*